© 2018. Published by The Company of Biologists Ltd | Journal of Experimental Biology (2018) 221, jeb168773. doi:10.1242/jeb.168773

RESEARCH ARTICLE

Turbulent flow reduces oxygen consumption in the labriform swimming shiner perch, *Cymatogaster aggregata*

Julie M. van der Hoop[1,‡], Margaret L. Byron[2,*], Karlina Ozolina[3], David L. Miller[4], Jacob L. Johansen[5], Paolo Domenici[6] and John F. Steffensen[7]

ABSTRACT

Fish swimming energetics are often measured in laboratory environments which attempt to minimize turbulence, though turbulent flows are common in the natural environment. To test whether the swimming energetics and kinematics of shiner perch, *Cymatogaster aggregata* (a labriform swimmer), were affected by turbulence, two flow conditions were constructed in a swim-tunnel respirometer. A low-turbulence flow was created using a common swim-tunnel respirometry setup with a flow straightener and fine-mesh grid to minimize velocity fluctuations. A high-turbulence flow condition was created by allowing large velocity fluctuations to persist without a flow straightener or fine grid. The two conditions were tested with particle image velocimetry to confirm significantly different turbulence properties throughout a range of mean flow speeds. Oxygen consumption rate of the swimming fish increased with swimming speed and pectoral fin beat frequency in both flow conditions. Higher turbulence also caused a greater positional variability in swimming individuals (versus low-turbulence flow) at medium and high speeds. Surprisingly, fish used less oxygen in high-turbulence compared with low-turbulence flow at medium and high swimming speeds. Simultaneous measurements of swimming kinematics indicated that these reductions in oxygen consumption could not be explained by specific known flow-adaptive behaviours such as Kármán gaiting or entraining. Therefore, fish in high-turbulence flow may take advantage of the high variability in turbulent energy through time. These results suggest that swimming behaviour and energetics measured in the lab in straightened flow, typical of standard swimming respirometers, might differ from that of more turbulent, semi-natural flow conditions.

KEY WORDS: Vortex, Eddy, Gait, Swimming kinematics, Metabolism, Space use

[1]Zoophysiology, Department of Bioscience, Aarhus University, 8000 Aarhus C, Denmark. [2]Department of Ecology and Evolutionary Biology, University of California Irvine, Irvine, CA 92697, USA. [3]Faculty of Biology, Medicine and Health, The University of Manchester, Manchester M13 9NT, UK. [4]Centre for Research into Ecological & Environmental Modelling and School of Mathematics & Statistics, University of St Andrews, Fife KY16 9LZ, UK. [5]Marine Biology Laboratory, New York University Abu Dhabi, PO Box 129188, Saadiyat Island, Abu Dhabi, United Arab Emirates. [6]CNR – IAMC, Istituto per l'Ambiente Marino Costiero, Località Sa Mardini, 09072 Torregrande, Oristano, Italy. [7]Department of Biology, University of Copenhagen, 3000 Helsingør, Denmark.
*Present address: Department of Mechanical and Nuclear Engineering, The Pennsylvania State University, University Park, PA 16802, USA.

‡Author for correspondence (jvanderhoop@bios.au.dk)

J.M.v.d.H., 0000-0003-2327-9000; M.L.B., 0000-0001-8012-078X; K.O., 0000-0002-7351-7372; D.L.M., 0000-0002-9640-6755; J.L.J., 0000-0001-8475-0447; P.D., 0000-0003-3182-2579; J.F.S., 0000-0002-4477-8039

Received 22 August 2017; Accepted 21 March 2018

INTRODUCTION

The complex habitats in which many marine organisms live are governed by stochastic, multiscale processes. However, unpredictability is often purposefully limited in studies of fish–flow interaction. Water tunnels, flumes and other apparatus are usually fitted with honeycombs or grids that straighten flow streamlines and minimize turbulent velocity fluctuation (Bainbridge, 1958; Bell and Terhune, 1970; Webb, 1975; Steffensen et al., 1984; Hove et al., 2000; Drucker and Lauder, 2002).

In the interest of mimicking the natural environment, recent laboratory experiments have sought to explore the relationship between fish and more complex flows (as reviewed in Liao, 2007). Flows have been altered via the introduction of boulders (Shuler et al., 1994) and logs (McMahon and Hartman, 1989); Plexiglas structures (Fausch, 1993); cones, spheres and half-spheres (Sutterlin and Waddy, 1975); horizontally or vertically oriented circular cylinders (Sutterlin and Waddy, 1975; Webb, 1998; Montgomery et al., 2003; Cook and Coughlin, 2010; Tritico and Cotel, 2010); and D-section cylinders (Liao, 2003, 2004, 2006; Taguchi and Liao, 2011). Other researchers have introduced fluctuations in water flow speed (Enders et al., 2003; Roche et al., 2014) or body-scale streamwise vortices (Maia et al., 2015). All these methods have served to introduce regular hydrodynamic perturbations in otherwise straightened flows, providing a more realistic approximation of the natural habitat of the animals studied. In some specific cases, the consistent flow features produced by these perturbations are exploited by fish to reduce the metabolic cost of swimming (Enders et al., 2003; Liao, 2004).

The response of fish to these 'altered' or complex flows (i.e. non-turbulent but vortex perturbed) can be highly variable (e.g. Cotel and Webb, 2012). It has been hypothesized that swimming in unsteady flows increases energy consumption by requiring additional swimming manoeuvres (Blake, 1979; Weatherley et al., 1982; Puckett and Dill, 1984; Webb, 1991; Boisclair and Tang, 1993; Maia et al., 2015). While some studies have shown that fluctuating flows reduce maximum swimming speed (Pavlov et al., 2000; Tritico and Cotel, 2010; Roche et al., 2014) and increase energy expenditure (Enders et al., 2003; Maia et al., 2015), other studies have found no effect of flow variability on performance metrics in a variety of species (Ogilvy and DuBois, 1981; Nikora et al., 2003). The effects of complex flows on fish swimming performance and oxygen consumption rate are dependent on the magnitude of the turbulence/velocity fluctuations (Pavlov et al., 2000; Lupandin, 2005; Tritico and Cotel, 2010; Webb and Cotel, 2010; Roche et al., 2014) and are probably tied to the fish's swimming behaviour [body–caudal fin (BCF) versus median–paired fin (MPF)]. Swimming performance may also be improved if fish can sense and respond to periodic vortex structures (Liao, 2007). However, these controlled situations may not be

Journal of Experimental Biology (2018) 221, jeb168773. doi:10.1242/jeb.168773

directly comparable to many natural habitats in which fish live, where aperiodic components of the flow can be dominant.

It is important to note that many of these 'altered' flows do not fit the classical definition of turbulence; they include strong periodic components and little stochasticity, which is a key feature of turbulence (Tennekes and Lumley, 1972; Pope, 2000). In the biological literature, turbulence is described as 'highly irregular' (Vogel, 1994) and 'chaotic' (Denny, 1993). Therefore, turbulence should be distinguished from highly periodic coherent structures such as waves or vortex streets. These structures may be influenced by turbulence or have turbulence superimposed upon them, but are not themselves 'turbulent'.

How fish respond to unstraightened, irregular flows in a swimming respirometer, as compared with the straightened and fluctuation-minimizing flows often used in laboratory experiments, is largely unknown. In most previous studies involving 'altered' flows (above), periodic fluctuations were introduced by adding features to otherwise straightened flows. In the present study, an unstraightened flow was compared with a standard, straightened flow. In both flows, energy was introduced by an impeller, and the resulting turbulence was allowed to decay over the length of the respirometer. In the unstraightened (high-turbulence) condition, flow was unimpeded from the impeller to the working section, save for a large-opening grid that served to confine the animal to the working section of the swim tunnel (the section to which the fish is confined when swimming; Ellerby and Herskin, 2013). Animals in the working section therefore encountered a field of aperiodic vortices and eddies which remained large relative to the size of the chamber. In the straightened (low-turbulence) condition, the flow features were quantifiably reduced in size via the inclusion of a honeycomb flow straightener and subsequent fine-mesh grid. The flow straightener included tubes with a sufficiently small diameter to damp out velocity fluctuations and eliminate large eddies before they are advected into the test section (Seo, 2013). In the unstraightened flow, turbulence intensity, turbulent kinetic energy, dissipation rate and other metrics were substantially increased relative to the straightened flow. These two configurations produced two distinct conditions: high-turbulence flow (HTF) and low-turbulence flow (LTF).

The metabolic cost of swimming in these two flows was examined, and the swimming kinematics were compared between the two conditions. Although previous studies have shown variable effects of turbulence on the metabolic cost of swimming (e.g. Pavlov et al., 2000; Lupandin, 2005; Tritico and Cotel, 2010; Webb and Cotel, 2010; Roche et al., 2014), it was expected that oxygen consumption rates would be greater in HTF compared to LTF, because of additional postural control and unsteady motion necessary to respond to aperiodic fluctuations in the flow field.

MATERIALS AND METHODS

Particle image velocimetry (PIV)

Setup and imaging technique

PIV was used to investigate and quantify turbulence in the swim-tunnel respirometer (Fig. 1). The vertical midplane of the working area was illuminated by a 1 W laser of wavelength 445 nm, spread into a thin sheet via a rigidly attached cylindrical lens (S3 Spyder III Arctic, Wicked Lasers, Shanghai, China; Fig. 1). At speeds >0.30 m s^{-1}, images of the vertical midplane were collected at 872 Hz with an exposure time of 1146 µs, using a high-speed, high-resolution camera (HHC Mega Speed PRO X4, Mega Speed, San Jose, CA, USA).

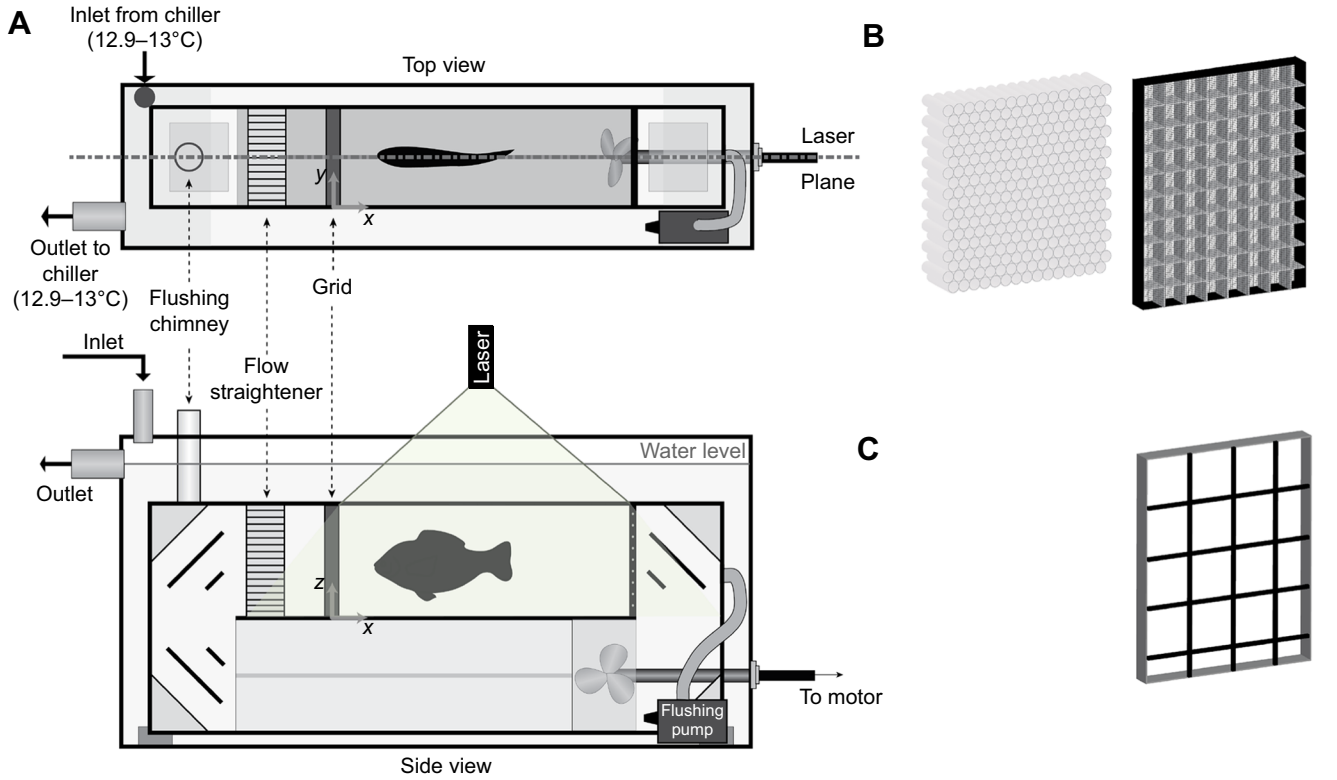

Fig. 1. Experimental setup. (A) Diagram of top and side views of the experimental setup, shown for the low-turbulence flow (LTF) condition with the flow straightener present. The laser plane (top view, dot–dash line) was used for particle image velocimetry (PIV) measurement. The flow straightener was not included in the high-turbulence flow (HTF) condition. (B) Flow straightener and fine-mesh grid used for filtering out large eddies for the LTF condition. (C) Large-opening grid used to restrain fish in the HTF condition, with no flow straightener.

At speeds <0.30 m s^{-1}, images were collected at 500 Hz with an exposure time of 2000 µs. Image resolution was 1280×720 pixels at higher speeds and 1280×1024 pixels for lower speeds.

The flow was seeded with hydrated *Artemia* cysts (Sanders' Premium Great Salt Lake *Artemia* Cysts) at an approximate seeding density of 16 cm^{-2} throughout the illuminated midplane. To ensure neutral buoyancy of the tracer particles, dry *Artemia* cysts were mixed into beakers of seawater at approximately 40 g l^{-1}, and left undisturbed for a minimum of 40 min to allow positively or negatively buoyant particles to rise or fall out of suspension (Lauder and Clark, 1984). Positively buoyant particles were skimmed from the water surface, and suspension containing near-neutrally buoyant particles was removed and added to the swim-tunnel respirometer. *Artemia* cysts from the Great Salt Lake strain are known to have a mean diameter of approximately 250 µm (Vetriselvan and Munuswamy, 2011), which in the camera view corresponds to approximately 1 pixel. Light scattering from these tracers increased the average diameter seen in the camera view to 2–3 pixels, as is appropriate for PIV (Melling, 1997; Raffel et al., 2007).

Image analysis

Images were batch processed in Adobe Photoshop to adjust balance and enhance contrast before performing vector computation via two-pass iteration in DaVis (LaVision GmbH, Goettingen, Germany). Subwindows were 64×64 pixels (13.4×13.4 mm) and 32×32 pixels (6.7×6.7 mm) with 50% overlap, resulting in flow resolved to 3.3 mm. This is sufficient to examine the scales of interest, as flow structures smaller than 3.3 mm are not likely to affect fish of the size used in this experiment (Tritico and Cotel, 2010). Vectors were computed for the entire working area in both HTF and LTF.

Flow characterization

Several of the many parameters available to describe the level of variability in turbulent flows (Cotel and Webb, 2012) were calculated for both HTF and LTF. These parameters are defined and described in detail in Table S1. They are u_T, the turbulent velocity scale; TKE, the turbulent kinetic energy; TI, the turbulence intensity; ω_y^2, the enstrophy (the square of vorticity); ε, the energy dissipation rate; L_{xx} and L_{zz}, the integral length scales in x and z; λ, the Taylor microscale; and η, the Kolmogorov microscale. All parameters (with the exception of the integral length scales and spectra) were calculated as spatiotemporally varying quantities, defined at each x–z point for each frame (where a frame is one PIV image pair). Quantities were averaged in time to calculate mean quantities, with 95% confidence intervals calculated via bootstrapping in time (approximately 6 s per flow speed and turbulence condition, with 8 data points calculated throughout the range of tested speeds). The outer 2 cm of each frame (close to the grid and walls) was not included in the averages to avoid including the effects of boundary layers. Integral length scales were found by calculating the appropriate autocorrelations in x and z. Throughout the manuscript, we use u to represent the spatiotemporally varying fluid velocity, whereas U represents the swimming speed of the fish (equivalent to the mean fluid velocity across the tunnel).

Flow properties

Non-overlapping 95% confidence intervals (CIs) indicated that HTF had significantly higher average values of TKE, TI, ω_y^2 and ε compared with LTF (Fig. S1), across the range of tested flow speeds. The difference between HTF and LTF generally increased with flow speed: TKE, ω_y^2 and ε all increased with flow speed in HTF, but in LTF, these parameters remained low and relatively constant despite the increasing flow speed. TI was higher in HTF than in LTF but was highest at low speeds and reached a plateau as speed increased (0–0.4 m s^{-1}; Fig. S1D). This was expected, as TI represents the ratio of fluctuations to mean flow; as mean flow increases, fluctuations will become stronger and TI will remain constant.

At high speeds, TI was approximately 150% higher in HTF than in LTF. At the highest tested speed, TKE was 500% higher in HTF, ω_y^2 was 170% higher and ε was 370% higher. For the difference in turbulence properties across the full range of flow speeds tested, see Fig. S1. The turbulence properties observed in the laboratory-generated flow (in both HTF and LTF) were comparable to those that would be experienced by *C. aggregata* in its natural habitat of coastal estuaries, bays and streams (see Table 1).

Three turbulent length scales were calculated to illustrate the differences in eddy size between HTF and LTF. The Taylor microscale λ (representing the average distance between stagnation points within the flow) and streamwise integral length scale L_{xx} (representing the overall average eddy size) were both larger in HTF than in LTF, and the Kolmogorov scale η was generally smaller in HTF (Fig. S2). [We note that the Kolmogorov scale in our experiments, averaging approximately 0.2–0.4 mm, is aligned with the expected values for small-scale ocean turbulence (0.3–2 mm; Jiménez, 1997). However, it is not possible to match the larger length scales to the animal's natural habitat. In an experimental context, these larger length scales are bounded by the respirometer's overall size and therefore cannot approach the wind- and tide-driven scales typical of the coastal ocean.] The relative sizes of these three scales signify that in HTF, fish were swimming through a larger range of spatial scales within the flow. Additionally, the vorticity field suggests differences in overall flow structure between the two flow conditions (Fig. 2). To verify that the flow did not contain any significant periodic components, the frequency spectra of both HTF and LTF were calculated throughout the tested velocity range (Fig. S3). No discrete periodicity, such as that produced by vortex shedding or driven by the flow impeller, was observed within the working section, and the spectra were consistent with classic turbulent spectra showing an energetic cascade from low to high frequencies. As expected, HTF contained more energy overall across all frequencies (Fig. S3).

Table 1. Turbulence parameters from this study as compared with field-measured quantities from the coastal habitats of shiner perch, *Cymatogaster aggregata*

	Current study		
Property	LTF	HTF	Natural habitat
ω_y^2 (s^{-1})	2–23	4–62	4–6400 surf zone 0–25 inlets and estuaries (Fuchs and Gerbi, 2016)
ε (m^2 s^{-3})	$10^{-4.5}$–$10^{-3.5}$	$10^{-4.2}$–$10^{-2.8}$	$10^{-3.5}$–10^{0} intertidal (Gaylord et al., 2013) $10^{-7.2}$–10^{-3} coastal bay with waves (Jones and Monismith, 2008)
TKE	$10^{-4.7}$–$10^{-3.7}$	$10^{-4.1}$–$10^{-2.9}$	10^{-4}–10^{0} tidal channel (Guerra and Thomson, 2017)

Data from this study are for both low-turbulence flow (LTF) and high-turbulence flow (HTF) conditions. ω_y^2, enstrophy (square of vorticity); ε, energy dissipation rate; TKE, turbulent kinetic energy.

Journal of Experimental Biology (2018) 221, jeb168773. doi:10.1242/jeb.168773

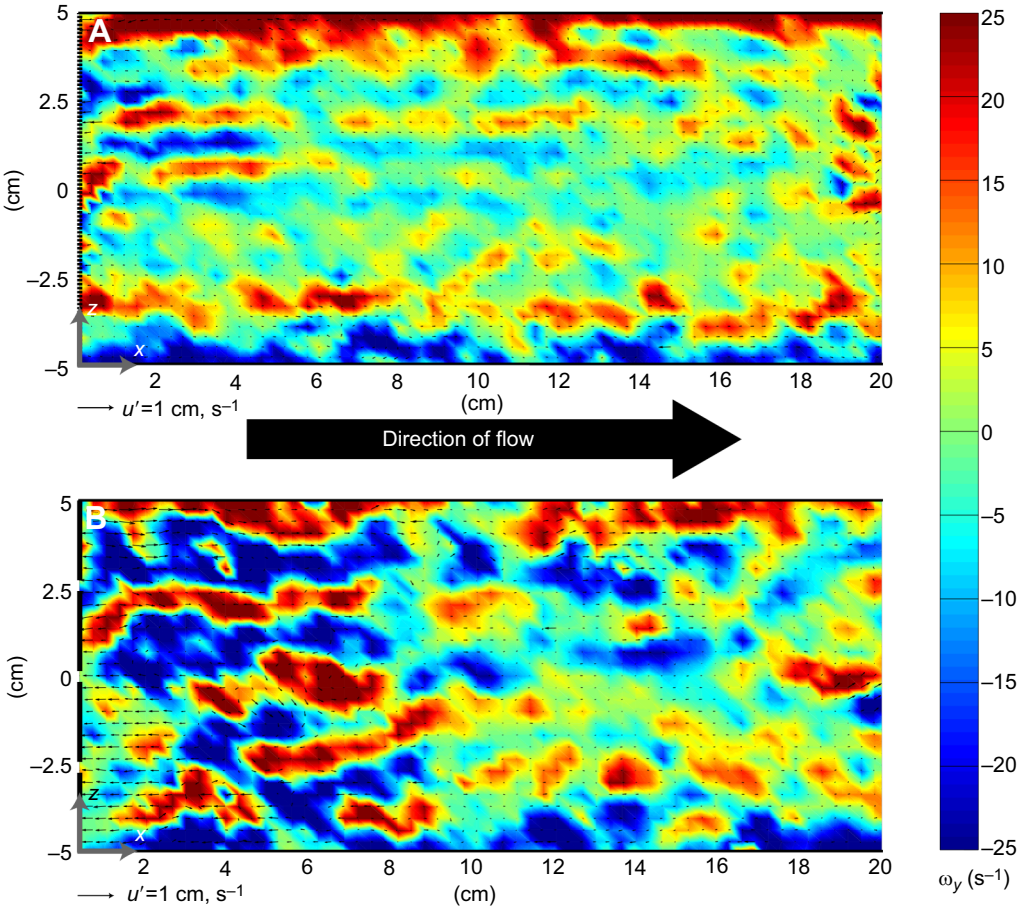

Fig. 2. Sample vector fields of the lateral view of the test section. Data are shown for the (A) LTF and (B) HTF conditions at the same mean streamwise velocity (0.38 m s^{-1}). Mean streamwise velocity has been subtracted to reveal coherent structures; the colormap shows vorticity (ω_y), overlaid by the instantaneous fluctuating velocity component u' (defined as u, the spatiotemporally varying component, minus $\bar{u}$, the overall mean velocity). Direction of flow is from left to right, with the top and bottom of the swimming chamber qualitatively represented by solid black lines and the two different grids on the left, represented by black dashed lines.

To summarize, two different flow conditions were created in a swimming respirometer. Both of these flows are turbulent, containing aperiodic velocity fluctuations. Neither flow contains large, periodic coherent structures (such as the von Kármán vortex street typically shed from a bluff body; Fig. S3). However, HTF is measurably more turbulent than LTF: it has larger velocity fluctuations at a given speed (higher TI), dissipates energy at a higher rate (ε) and contains a larger variance of eddy sizes (L_{xx}, L_{zz}, λ, η) as well as stronger extremes of vorticity ($\omega_y{}^2$; Figs S1 and S2). Therefore, a significant difference was expected in the energetics of fish swimming in these two flow conditions.

Fish collection and husbandry

Shiner perch, *Cymatogaster aggregata* Gibbons 1854, were collected by beach seine at Jackson Beach, San Juan Island, WA, USA (48°31′N, 123°01′W) in July and August 2013. Fish body length (BL, mean±s.d.) measured 12.1±0.3 cm, and mass was 40±7.1 g. Fish were kept in 120×56×15 cm and 90×59×30 cm tanks with recirculating seawater at the University of Washington's Friday Harbor Laboratories, and they fed on plankton present in the water. Fish were fasted for a minimum of 4 h prior to experimental trials. Ambient seawater temperature followed ocean conditions of the area and ranged from 12 to 14°C. After capture, individuals were maintained in aquaria for at least 3 days before their first experimental trial, and were given a minimum of 2 days to recover between trials. Eight fish that performed trials in both the low- and high-turbulence conditions were used for analysis. The order of low- and high-turbulence exposure was randomized for each individual by flipping a coin.

Swimming energetics

Experiments were conducted in an 8.31 l clear Steffensen Model 1 Plexiglas swimming respirometer with a working section of 9.0×26.0×11.0 cm (width×length×depth, w×l×d). LTF and HTF were induced by inserting two different grid conditions (Fig. 1). For LTF, the tunnel was fitted with a 9.4×10.6×3.3 cm (width×depth×thickness, w×d×t) honeycomb straightener (0.6 cm tube diameter) followed by a 0.01 cm^2 square mesh mounted on a 9.2×11.9×1.7 cm (w×d×t) plastic grid (1.2×1.2 cm opening size). This fine mesh reduced the size of the incoming coherent flow structures, further straightening the flow. For HTF, the tunnel was fitted with a 9.2×11.8 cm (w×d) large-opening grid [opening size 2.45×2.65 cm (l×h), coated wire thickness 2.7 mm on average]. These large openings constrained the fish to the desired test section while still allowing relatively large eddies (approximately 60% of fish body depth) to enter the test section. The honeycomb straightener was not present in the HTF regime.

Flow speed within the working section was driven by an impeller attached to an AC motor and motor control (DRS71S4/FI and Movitrac LTE-B B0004 101-1-20, respectively; SEW Eurodrive, Wellford, SC, USA), and was calibrated prior to experiments with a Höntzsch TAD W30 flow-meter (Höntzsch, Waiblingen, Germany). Flow speed is hereafter reported in body lengths per second (BL s^{-1}). Water temperature during trials was maintained between 12.9 and 13.0°C by an external chiller.

Before each trial, fish were acclimated in the test section for a minimum of 4 h (maximum 8 h 53 min), swimming at 0.5 BL s^{-1}. After acclimation, speed was increased by 0.5 BL s^{-1} every 30 min up to a maximum of 4.5 BL s^{-1} (the maximum speed reached by

Journal of Experimental Biology (2018) 221, jeb168773. doi:10.1242/jeb.168773

any fish; maximum of 9 speed measurements in total for a given fish). Solid blocking effects were accounted for based on criteria established by Bell and Terhune (1970). Each fish performed LTF and HTF trials in a randomized order; the time of day of the two trials was held constant for a given fish to eliminate potential effects of photoperiod on fish metabolism and allow direct comparison between HTF and LTF for the same individual. The rate of oxygen consumption ($\dot{M}_{O_2}$; mg O_2 kg^{-1} h^{-1}) was obtained through intermittent flow respirometry (Steffensen, 1989). Oxygen was measured with a PreSens Fibox 3 fibre optic oxygen meter (PreSens, Regensburg, Germany) inserted into the flushing chimney, and $\dot{M}_{O_2}$ was calculated in LoliRESP as described in Steffensen (1989). Three oxygen determinations were made at each swimming speed, with 180 s flush, 120 s wait and 600 s measurement periods comprising a 15 min cycle (Svendsen et al., 2016). Following each trial, oxygen consumption was measured in the closed, empty respirometer to obtain background bacterial respiration rates. The measured bacterial respiration was then subtracted from all $\dot{M}_{O_2}$ measurements in that trial. Bacterial respiration was not measured for two trials (fish 5 LTF, fish 13 HTF); in those cases, the average bacterial respiration from all other trials was subtracted from total measured $\dot{M}_{O_2}$.

Kinematics and space use

All swimming kinematics, including both fin beat frequencies and fish position within the working section, were filmed at 30 frames s^{-1} with a tripod-mounted Casio Exilim EX-FH100 camera filming horizontally. A mirror was placed above the respirometer's working section at 45 deg to provide simultaneous lateral and aerial views of the swimming fish, similar to the schematic diagram shown in Fig. 1. Kinematics were measured at three distinct swimming speeds: low (0.5 BL s^{-1}), medium (1.5 BL s^{-1}) and high (shared maximum velocity, U_{max}; range 3.5–4.5 BL s^{-1}, mean 3.9 BL s^{-1}). High swimming speed is defined as the shared U_{max}, being the highest flow velocity attained by a given individual before fatigue in both low- and high-turbulence trials (e.g. if a fish attained 3.5 BL s^{-1} in LTF and 4.0 BL s^{-1} in HTF, the shared U_{max} is 3.5 BL s^{-1}). Fatigue was defined as when a fish could no longer swim unassisted and rested against the back grid for >5 s; a speed level was 'attained' if a fish performed all flushing cycles at that flow speed. These three levels were chosen to illustrate swimming kinematics throughout a range of speeds and to simplify analyses relative to the more highly resolved $\dot{M}_{O_2}$ analysis.

Spatial position

The 3D position coordinates $\rightarrow x = (x_s, y_s, z_s)$ of the tip of the snout of each fish were digitized in Tracker v.4.81 (http://physlets.org/tracker/). Coordinates were digitized every 10 frames (equivalent to 3 frames s^{-1}) for the last 180 s of the second (of three) 600 s measurement periods. For each trial, the centroid (x_c, y_c, z_c) and standard deviation of the 3D snout coordinate (x_s, y_s, z_s) were calculated for each trial, with the standard deviation reflecting some measure of variance overall (e.g. Fig. 3).

Pectoral fin and tail beat frequency

Pectoral and caudal fin use were determined from video footage at the previously defined low, medium and high flow velocities. The time of adduction of the pectoral fin and of complete cycles of left and right displacement of the caudal fin was recorded (e.g. Drucker and Jensen, 1996). We calculated the pectoral and caudal fin beat frequencies (Hz) as the reciprocal of the mean waiting time between

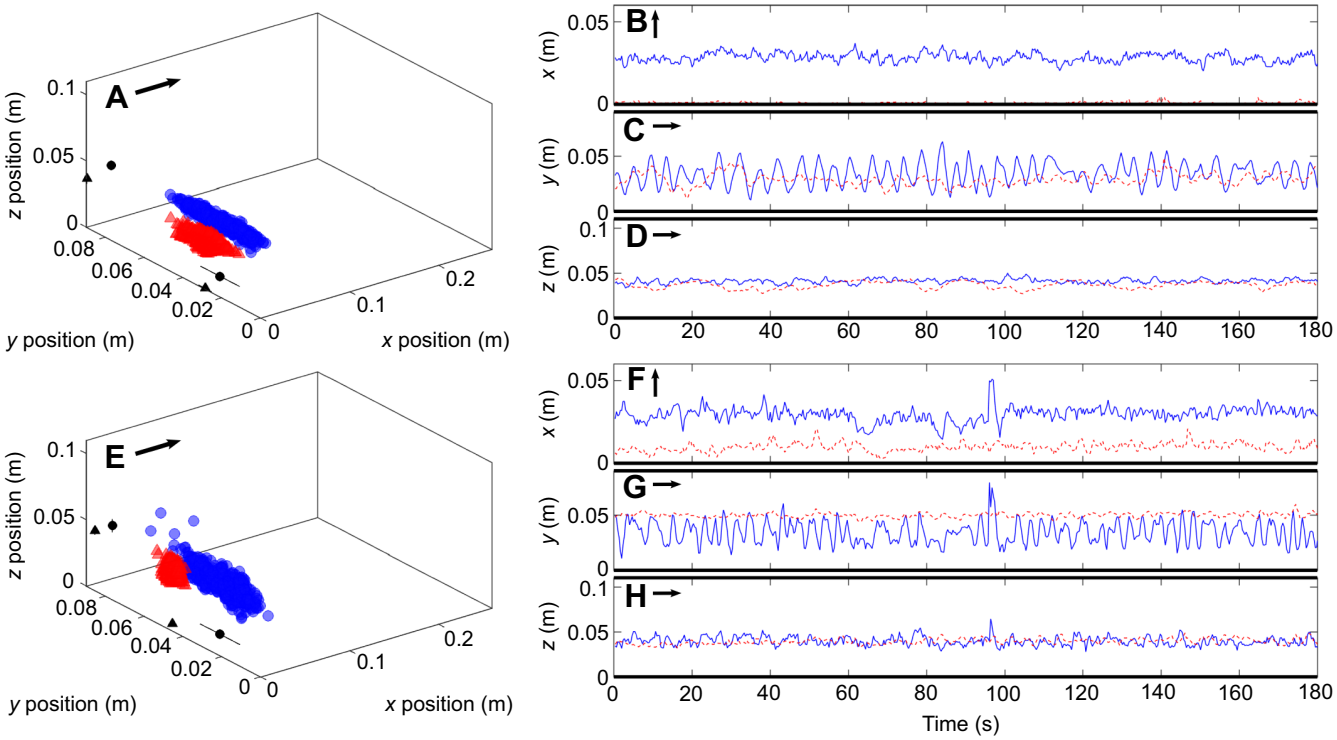

Fig. 3. 3D position of one fish in a swimming respirometer in LTF and HTF conditions. All snout positions (x_s, y_s, z_s; coloured symbols), centroid positions (x_c–y_c and x_c–z_c; black symbols) and standard deviation (black lines) of one sample fish swimming in LTF (red) and HTF (blue) at 1.5 BL s^{-1} (A–D) and 4.0 BL s^{-1} (E–H), along with time series of x_s, y_s and z_s (B–D, F–H) are shown. The x=0 position represents the location of the grid in both LTF and HTF. Thicker lines represent the location of the tank walls, and arrows indicate flow direction (see also Fig. 1).

Journal of Experimental Biology (2018) 221, jeb168773. doi:10.1242/jeb.168773

beats (1/mean difference in beat time) over the 180 s measurement period (Fig. S4). The gait transition speed (U_{pc}) in *C. aggregata* (12 cm) has been reported to be ∼3.5 BL s^{-1} (e.g. Mussi et al., 2002) and we observed some use of the caudal fin, in line with previous work. However, a transition to exclusively caudal fin locomotion was not observed in any fish.

Statistical analyses

Swimming energetics

Non-linear mixed effects models fitted by restricted maximum likelihood (using nlme in nlme; https://CRAN.R-project.org/package=nlme) were used to compare the relationship between $\dot{M}_{O_2}$ (mg O_2 kg^{-1} h^{-1}) and speed (U; BL s^{-1}) between individual fish under different turbulence conditions (see Script 1; R version 3.4.1, https://www.r-project.org/). Following Roche et al. (2014), we fitted a model of the functional form:

$$\dot{M}_{O_2} = a + bU^c. \quad (1)$$

For each of a, b and c, two parameters were estimated, one for each condition (for a total of 6 fixed effects parameters). A random effect was used to account for per-fish variation. Visual inspection of residuals against fish and speed revealed no issue with heteroscedasticity. Plots of observed versus fitted values showed good agreement between the data and model (Script 1; Zuur et al., 2010). A *post hoc* paired t-test was used to detect differences in $\dot{M}_{O_2}$ between conditions at each speed, with a false discovery rate correction for multiple comparisons (Benjamini and Hochberg, 1995).

Kinematics and space use

To assess how $\dot{M}_{O_2}$ changed with fin beat frequency, we fitted a generalized additive model (Wood, 2017) to the $\dot{M}_{O_2}$, using pectoral or caudal fin beat frequency (Hz) as separate explanatory variables. We used factor–smooth interactions (Baayen et al., 2018) to fit two levels of a smooth function of measured beat frequency, one for each flow condition. Such terms fit the base level of the factor as a smooth, then model deviations from that smooth for the other level; thus, information was shared between the models while allowing for a flexible relationship that makes no assumptions about functional form. Fish ID was included as a random effect. Models were fitted by restricted maximum likelihood.

Goodness of fit for the generalized additive model of oxygen consumption as a function of pectoral fin beat frequency was assessed using standard plots (Wood, 2017). The factor–smooth interaction was sufficiently flexible to model the shape of the relationship (6.489 effective degrees of freedom, given a maximum basis complexity of 20), deviance residuals appeared to be approximately normal and showed little pattern with increasing values of the linear predictor (hence did not have an issue with heteroscedasticity), and the relationship between fitted and observed values of $\dot{M}_{O_2}$ was approximately linear. The random effect for fish ID approximated normal from a Q–Q plot.

We attempted to fit a similar model to the relationship between oxygen consumption and caudal fin beat frequency; however, the model fit was unsatisfactory as 64.6% of the time the fin beat frequency was recorded as zero, limiting model fitting options. Given the poor fit of our model, we do not present any modelling results for caudal fin beat frequency but present the raw data in Script 1.

Following Kerr et al. (2016), we visualized the 3D position of all fish in each flow and speed condition with heatmaps, to determine whether fish were consistent in their positions in HTF or LTF, perhaps to take advantage of regional flow conditions or 'dead spots'. To aid interpretation of the results, we plotted the standard deviation of position per fish, flow condition and speed and fitted a rudimentary linear model per fish and flow condition (Script 1).

To determine the relationship between fish swimming kinematics, energetics and ambient flow, the frequency components of the fish's x–y–z position within the respirometer were analysed. This analysis was undertaken to further ensure that any periodic position fluctuations displayed by the fish were not a result of variables related to the surrounding flow (i.e. condition or speed); that is, that periodic position fluctuations were not indicative of fish using vortex structures to save energy. Periodicity in the time series of (x_s, y_s, z_s) (e.g. Fig. 3B–D,F–H) was detected for each fish with Fisher's g-statistic above 0.1 Hz as a result of the 3 frames s^{-1} sampling frequency (Wichert et al., 2004). Space-use analyses were completed in MATLAB (R2011a-R2014b, MathWorks, Inc., Natick, MA, USA).

RESULTS

Swimming energetics

The power functions describing the relationship between $\dot{M}_{O_2}$ and swimming speed (Fig. 4) were, for LTF:

$$\dot{M}_{O_2} = 167.2 \pm 8.2 + 5.0 \pm 1.2U^{2.9\pm0.2} \quad (2)$$

and for HTF:

$$\dot{M}_{O_2} = 156.7 \pm 6.4 + 6.4 \pm 2.4U^{2.2\pm0.3}. \quad (3)$$

Bacterial $\dot{M}_{O_2}$ ranged from 1.8 to 6.6 mg O_2 h^{-1}. The standard deviation of the fish ID random effect, i.e. the intercept (equivalent to standard metabolic rate), was 30.46 mg O_2 kg^{-1} h^{-1}.

At 0.5 BL s^{-1}, fish in the HTF condition consumed 10.5±6.4 mg O_2 kg^{-1} h^{-1} (66%) less than when in the LTF condition (167.2±15.6 mg O_2 kg^{-1} h^{-1}). The exponent of the relationship was significantly different between these flow conditions (t_{369}=−2.328, P=0.0204); differences between treatments occurred at speeds >2 BL s^{-1}. $\dot{M}_{O_2}$ was not significantly different between LTF and HTF at speeds below 1.5 BL s^{-1} (paired t-test with false discovery rate correction, F_7<1.889, P>0.13; Fig. 4). Fish

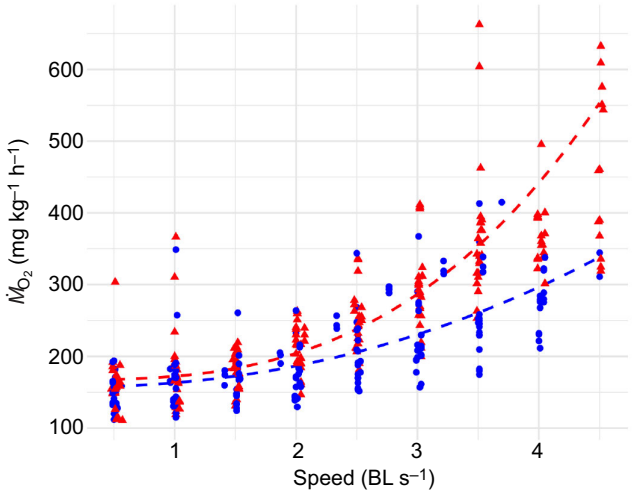

Fig. 4. Mean oxygen consumption rate ($\dot{M}_{O_2}$) is significantly higher in LTF than in HTF conditions at swimming speeds >2 BL s^{-1}. Symbols represent $\dot{M}_{O_2}$ measurements for each fish (n=8) at each speed and condition (red, LTF; blue, HTF). Dashed lines represent fitted curves.

Journal of Experimental Biology (2018) 221, jeb168773. doi:10.1242/jeb.168773

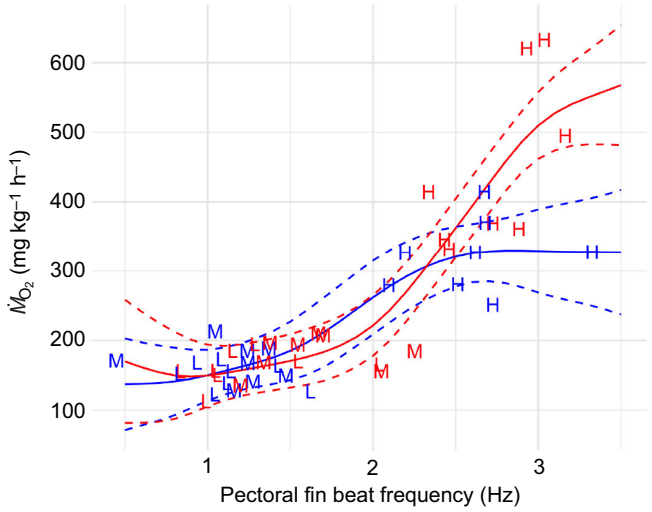

Fig. 5. $\dot{M}_{O_2}$ increases with pectoral fin beat frequency in LTF and HTF conditions. Predicted oxygen consumption is shown as a function of pectoral fin beat frequency in *n*=8 shiner perch (solid lines), along with 95% confidence intervals (dashed lines). Data are shown as letters (red, LTF; blue, HTF) indicating the flow speed [L, low, 0.5 BL s^{-1}; M, medium, 1.5 BL s^{-1}; H, high, shared maximum velocity (U_{max}), 3.5–4.5 BL s^{-1}]. The observed value of fish ID is conditioned on the predictions. Confidence bands are wider at either end of the plot range as there are no data beyond the range and there is greater uncertainty about the shape of the smooth when there are no previous/further data.

consumed significantly less (on average 20% less, range 0–46%) O_2 in HTF versus LTF conditions at speeds above 2.0 BL s^{-1} (F_7>3.038, P<0.03; Fig. 4).

Kinematics and space use

As expected (e.g. Roche et al., 2014), predicted $\dot{M}_{O_2}$ monotonically increased with pectoral fin beat frequency (Fig. 5) in both flow conditions. The factor–smooth interaction showed significant divergence between the two flow conditions when the fin beat frequency was above 2.75 Hz, as evidenced in the difference in 95% CIs (±2 standard errors from the smooths of fin beat frequency; Fig. 5).

Overall space use in the tank was visualized using heatmaps, following Kerr et al. (2016), which did not suggest consistent positioning in the tank between fish and in different flow and speed conditions (Fig. 6). The centroid positions in x, y and z showed no consistent response to speed or flow condition (Script 1). In both flow conditions in the x- and y-directions, deviation decreased with increasing speed. In the x- and y-directions, deviation was greater in HTF than in LTF. For the z-direction, there was little difference in deviation between LTF and HTF conditions. Further, there was little effect of speed on deviation in HTF but a stronger effect of speed on deviation in LTF (Script 1). In combination with heatmaps (Fig. 6), this approach gives some idea of the behaviour of the fish in the tank. Overall, space use in LTF was constrained to a small area at the front of the working section. In HTF, fish position was spread across a larger area (Fig. 6).

Significant periodicity was detected in time series of x_s (1.81±2.95 Hz; mean±s.d.), y_s (1.57±0.76 Hz) and z_s (11.35±0.66 Hz), but in only a proportion of all cases (x=26/48, y=34/48, z=32/48).

DISCUSSION

Most studies of fish swimming and respirometry have used flow-straightening devices that result in low-turbulence flow conditions within the experimental setup, similar to the LTF condition described in this study. The natural habitat of most fishes is more turbulent than that created by such laboratory conditions, but most studies seeking to create more natural flows have focused on fish behaviour in coherent vortex structures, which represent only a small portion of the flows encountered by fish in their natural habitats (Lacey et al., 2012; Kerr et al., 2016). In predictable vortex-dominated flows, it is common for fish to display energy-saving behaviour (e.g. Kármán gaiting) as a result of the consistent nature of the periodic vortices (Liao, 2003; Liao et al., 2003). Few studies have explicitly tested the effect of aperiodic, more randomized flow on fish swimming energetics and kinematics. Of these, many have suggested that fish should expend more energy in unsteady flows (Enders et al., 2003; Lupandin, 2005; Tritico and Cotel, 2010) or show greater variation among individuals (Kerr et al., 2016), as each fish must accommodate the unique flow structures it encounters. In the experiments described herein, we compared oxygen consumption and swimming movements of fish in LTF (similar to a standard fish respirometry study) versus a HTF (mimicking a more natural turbulent environment). Fish displayed significantly reduced metabolic costs when swimming in HTF compared with LTF. No periodic components of the flow or swimming kinematics can account explicitly for these energy savings, suggesting that fish may also be able to exploit turbulent flows without discernible periodic wake formations.

Fish have been shown to reduce the energetic costs of swimming (or otherwise adapt to changes in ambient flow) in specific circumstances by employing behaviours such as (1) gait switching (Korsmeyer et al., 2002), (2) Kármán gaiting (Liao, 2003), (3) entraining (Webb, 1998), (4) bow riding (Newman and Wu, 1975; Taguchi and Liao, 2011), (5) tail holding (Kerr et al., 2016) and (6) wall holding (Kerr et al., 2016). Below, the present results are discussed in the context of expected fish behaviour under these different energy-reducing strategies to identify potential mechanisms behind the reduced metabolic costs measured in this study.

We found that $\dot{M}_{O_2}$ increased significantly more with pectoral fin use in LTF than in HTF, and caudal fin use was often absent in these MPF swimmers. At high speeds prior to exhaustion, many MPF swimmers such as *C. aggregata* and other labriform swimmers start complementing pectoral fin swimming with the caudal fin (i.e. at gait transition; Webb, 1973; Svendsen et al., 2010). Webb (1973) describes little-to-no caudal fin use in *C. aggregata* at speeds below 3.4 BL s^{-1}. Typically, at speeds of 3.5–3.85 BL s^{-1}, *C. aggregata* used occasional low-frequency, low-amplitude caudal fin beats (caudal fin pattern A; Webb, 1973). Above 3.85 BL s^{-1}, *C. aggregata* used 1–3 caudal fin beats in quick succession to maintain position in the swimming flume (burst–coast swimming; caudal fin pattern B; Webb, 1973), but this occurred over a short period of time, immediately prior to exhaustion. Therefore, the overall proportion of time the caudal fin is used even after initial recruitment of the caudal fin can remain low (Webb, 1973; this study); gait transition in other labriforms has been shown to involve initial occasional recruitment of the caudal fin before slowly developing to full and continuous burst–coast swimming (Cannas et al., 2006). In addition, the fish in our study were smaller (12.1 cm) than those used by Webb (1973; 14.3 cm), and therefore they are expected to start using the tail at a higher relative speed (in BL s^{-1}; Mussi et al., 2002) than that found by Webb (1973). Further experiments focusing on fin and muscle use (pectoral versus caudal fin and red versus white muscle; e.g. Gerry and Ellerby, 2014) in unpredictable flow regimes would better resolve the

Journal of Experimental Biology (2018) 221, jeb168773. doi:10.1242/jeb.168773

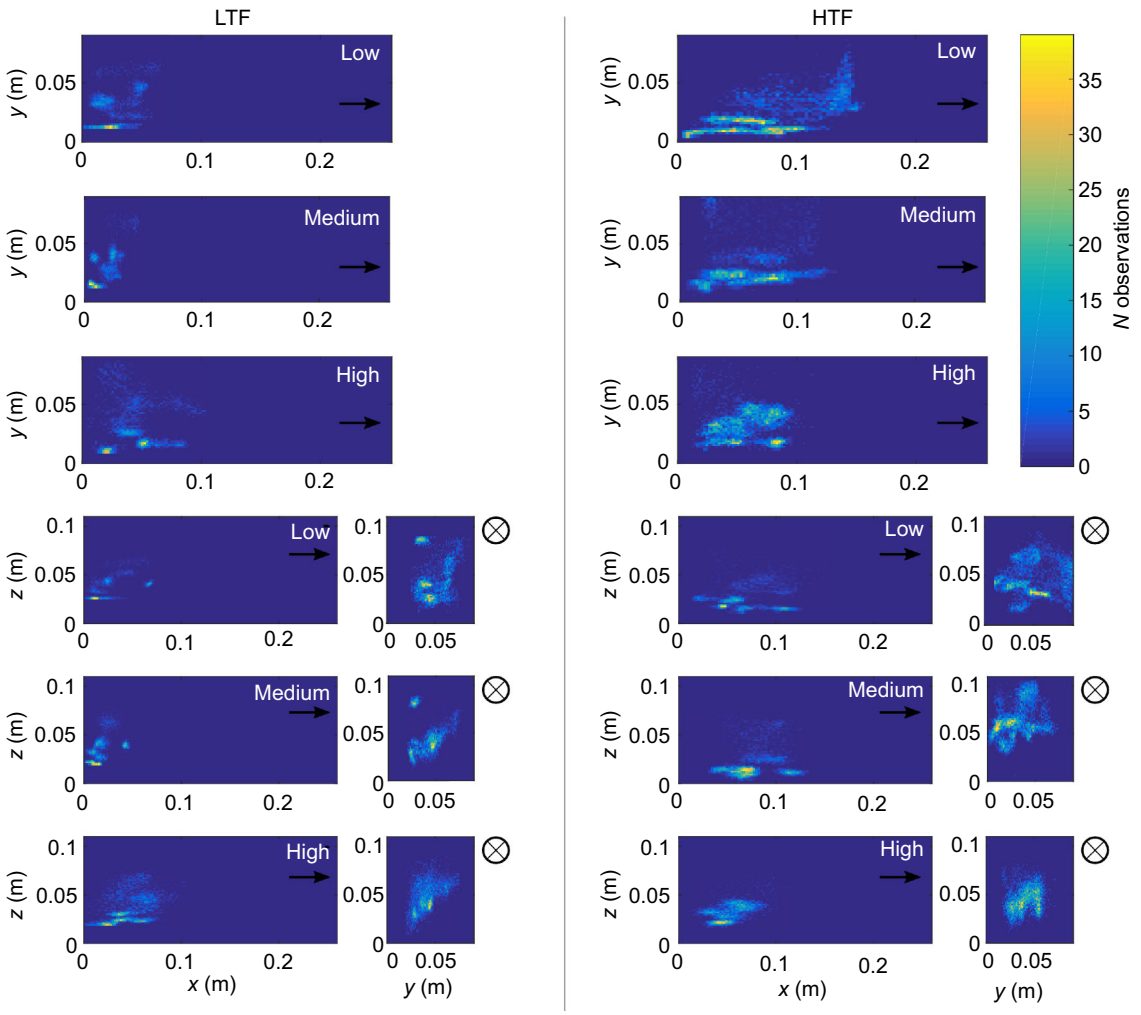

Fig. 6. Overall heatmap of space use in *x*-, *y*- and *z*-dimensions of *n*=8 shiner perch in a swimming respirometer in LTF and HTF conditions at different speeds. Low speed, 0.5 BL s^{-1}; medium speed, 1.5 BL s^{-1}; high speed, 3.5–4.5 BL s^{-1}. Arrows indicate flow direction, including flow into the page (circle with cross).

strength of the relationship between $\dot{M}_{O_2}$ and movement patterns and the mechanism behind different movements in complex flows.

Fish can reduce energetic expenditure by stationing behind a bluff body and altering their body kinematics to synchronize with shed vortices. This behaviour, called Kármán gaiting (Liao, 2003), requires the presence of a bluff body which can shed vortices of a size of the order of the fish's body depth (Tritico and Cotel, 2010); no such bluff body was available in the present experiments. The cross-tank body oscillation displayed by fish in HTF (e.g. Fig. 3) is at first glance suggestive of such a behaviour; however, this behaviour was not consistent between all fish, and the flow did not offer discrete periodicity (Fig. S3).

The orientation and/or size of vortices shed behind moving fins of MPF (*sensu* Webb, 1984) swimmers differs from that of BCF (*sensu* Webb, 1984) swimmers (Drucker and Lauder, 1999, 2002; Drucker et al., 2005; Fish and Lauder, 2006). Similarly, MPF swimmers maintain a rigid body during locomotion at speeds below gait transition and therefore would not be able to use energy-saving behaviour in the same manner as BCF swimmers, i.e. by synchronizing their tail beats with the vortex-shedding frequency (Kármán gaiting; Liao, 2003). Little is known about how MPF swimmers interact with vortices and turbulence in order to save energy. Interestingly, previous work has shown that, like BCF swimmers (Marras et al., 2015), MPF swimmers can save energy when swimming in the wake of neighbours in a school (Johansen et al., 2010). It is therefore possible that MPF swimmers exploit paired-fin motion kinematics and timing in order to minimize the energy spent on swimming in turbulent flow. Simultaneous kinematic measurements and PIV may better resolve the fine-scale movement responses of fish to moving flow structures.

Further energy-saving mechanisms often involve station holding either in front (i.e. bow riding; Taguchi and Liao, 2011) or behind (i.e. entrainment; Liao, 2006; Przybilla et al., 2010) bluff bodies, where fish use the resulting high-pressure zones or lift and wake suction forces, respectively, to maintain position. Fish have also been shown to tail hold by resting their tails against screens at the rear of experimental setups (Kerr et al., 2016). These behaviours cannot explain the reduced energy consumption observed in this study as there were no bluff bodies to station in front of, and fish generally stayed at the front of the respirometer, with their tails 5–15 cm from the rear grid (see Fig. 6). Fish can also display wall holding by potentially taking advantage of more stable and reduced flows in the wall boundary layer (Kerr et al., 2016). While overall space use (Fig. 6) shows that fish in this experiment had a slight preference for swimming on the left side of the respirometer, this positioning was dynamic in time. Fish moved back and forth across

the respirometer at higher flow velocities and in HTF (Fig. 3). Any spatial bias was therefore not likely to be due to standing flow features; that is, based on this movement pattern and PIV, there is no evidence of 'dead zones' of low flow where fish could consistently position themselves. In HTF, fish exhibited more movement across and along the test section (Fig. 6). A comparison of the movements of one fish (Fig. 3) and the heatmap of all fish (Fig. 6) shows individuals differ in their absolute position but that their positioning is consistently more variable in HTF. This could indicate a passive behaviour, i.e. fish are being advected back and forth by the larger turbulent eddies found in HTF, or an active behaviour, i.e. fish are exploiting temporary (not periodic) vorticity, which is higher in HTF than in LTF, to their advantage, in line with the lower $\dot{M}_{O_2}$ in HTF versus LTF conditions.

The results presented herein are not explained by previously described energy-saving mechanisms observed in fish. The fact that fish consume less oxygen when in more turbulent conditions may be the result of greater variability in their positions (compared with LTF), which in turn may help the fish to take advantage of the variability in turbulent energy through time and space observed in HTF. However, the mechanism by which this advantage is gained is not clear. The difference in energy consumption may also be due to the interplay between skin friction drag and pressure drag on a given fish. The Reynolds number of each fish ranged from approximately 5×10^5 to 5×10^6. This range is close to the 'drag crisis' regime, which is well studied in spheres and cylinders (Smith et al., 1999; Singh and Mittal, 2005; Kundu et al., 2011). In this regime, the boundary layer over the surface of a bluff body transitions from a laminar to a fully turbulent state, resulting in a smaller wake and lower pressure drag. In this case, the velocity fluctuations in HTF may 'trip' the boundary layer into the turbulent state, lowering the pressure drag compared with LTF. Further investigation of this possibility would require simultaneous PIV of the fish and flow.

The PIV analysis described here characterizes the flow and its eddies with no fish in the tank; the same analysis with the fish swimming simultaneously in the flume (e.g. Drucker and Lauder, 2002) was not possible because of (1) potential alteration of fish behaviour due to the laser light, (2) optical inaccessibility due to the presence of the animal and (3) animal welfare concerns over particulate density and non-infrared laser light. We were therefore unable to examine the specific flow structure for each individual and instead measured a 'representative' flow field in each condition (throughout the range of tested speeds) to be used for inference of all trials. Because of this, we cannot exclude the possibility that the presence of the fish created unique flow features, such as persistent zones of lower than average flow. However, if this were true, we would expect to see less-variable positioning in HTF as fish held station in these 'self-generated dead zones' to save energy. In fact, we found the opposite: less-variable position (and higher energy consumption) in LTF. Further understanding of the mechanism behind the observed behaviour could be achieved by conducting a similar experiment in which the fish kinematics, the flow field surrounding the fish and the fish's $\dot{M}_{O_2}$ were measured simultaneously.

Both turbulence and coherent vortex structures can have passive and active effects on fish, playing a role in postural control (Pavlov et al., 2000; Tritico and Cotel, 2010), foraging (MacKenzie and Kiørboe, 1995), transportation costs (Webb and Cotel, 2010; Webb et al., 2010), and orientation and swimming speed (Standen et al., 2004; Lupandin, 2005). It is critical that studies continue current research trends to determine the energetic, kinematic and behavioural effects of swimming in non-uniform, aperiodic flows that mimic the diversity of turbulence observed in habitats. In particular, this study has found that fish show significantly different patterns of positioning, kinematics and energetics in a typical laboratory flume (LTF) versus a more turbulent flow (HTF), at the highest flow velocities. Individual and context-specific responses to variable flows in terms of propulsive (Liao, 2003, 2004, 2007) or positioning strategies (herein) must be understood to better relate laboratory-based findings to natural environments (Roche et al., 2014). Whether the effects of turbulence on energy consumption are positive, neutral or negative (Enders et al., 2003), their quantification is essential in understanding the energetics of swimming in semi-natural, varying flow conditions (Cotel and Webb, 2015).

Acknowledgements
We would like to thank UW Friday Harbor Laboratories for their facilities, space and support for this project, Mega Speed for the loan of the high-speed camera, and E. A. Variano (UC Berkeley) for the loan of PIV laser equipment.

Competing interests
The authors declare no competing or financial interests.

Author contributions
Conceptualization: J.M.v.d.H., M.L.B., K.O., J.L.J., P.D., J.F.S.; Methodology: J.M.v.d.H., M.L.B., K.O.; Software: J.M.v.d.H., M.L.B., K.O.; Formal analysis: J.M.v.d.H., M.L.B., D.L.M.; Investigation: J.M.v.d.H., M.L.B., K.O.; Resources: J.J., P.D., J.F.S.; Writing - original draft: J.M.v.d.H.; Writing - review & editing: J.M.v.d.H., M.L.B., K.O., D.L.M., J.L.J., P.D., J.F.S.; Visualization: J.M.v.d.H., M.L.B.; Supervision: J.L.J., P.D., J.F.S.; Funding acquisition: J.M.v.d.H., M.L.B., K.O., P.D., J.F.S.

Funding
J.M.v.d.H. and M.L.B. were supported by Stephen and Ruth Wainwright Endowed Fellowships at UW Friday Harbor Laboratories. K.O. was supported by the Natural Environment Research Council, a Fisheries Society of the British Isles travel grant, and an Adopt-a-Student Program Scholarship at UW Friday Harbor Laboratories.

Data availability
Data and code related to the experiment and data analysis can be found at https://doi.org/10.5281/zenodo.1254101.

Supplementary information
Supplementary information available online at
http://jeb.biologists.org/lookup/doi/10.1242/jeb.168773.supplemental

References
Baayen, R. H., vam Rij, J., de Cat, C. and Wood, S. N. (2018). Autocorrelated errors in experimental data in the language sciences: some solutions offered by Generalized Additive Mixed Models. In *Mixed Effects Regression Models in Linguistics* (ed. D. Speelman, K. Heylen K. and D. Geeraerts), pp. 49-69. Berlin: Springer.

Bainbridge, R. (1958). The speed of swimming of fish as related to size and to the frequency and amplitude of the fail beat. *J. Exp. Biol.* **35**, 109-133.

Bell, W. H. and Terhune, L. D. (1970). *Water Tunnel Design for Fisheries Research*. Nanaimo, BC: Fisheries Research Board of Canada, Biological Station.

Benjamini, Y. and Hochberg, Y. (1995). Controlling the false discovery rate: a practical and powerful approach to multiple testing. *J. R. Stat. Soc. Ser. B* **57**, 289-300.

Blake, R. W. (1979). The energetics of hovering in the mandarin fish (*Synchropus picturatus*). *J. Exp. Biol.* **82**, 25-33.

Boisclair, D. and Tang, M. (1993). Empirical analysis of the influence of swimming pattern on the net energetic cost of swimming in fishes. *J. Fish Biol.* **42**, 169-183.

Cannas, M., Schaefer, J., Domenici, P. and Steffensen, J. F. (2006). Gait transition and oxygen consumption in swimming striped surfperch *Embiotoca lateralis Agassiz*. *J. Fish Biol.* **69**, 1612-1625.

Cook, C. L. and Coughlin, D. J. (2010). Rainbow trout Oncorhynchus mykiss consume less energy when swimming near obstructions. *J. Fish Biol.* **77**, 1716-1723.

Cotel, A. J. and Webb, P. W. (2012). The challenge of understanding and quantifying fish responses to turbulence-dominated physical environments. In *IMA 155: Natural Locomotion in Fluids and on Surfaces: Swimming, Flying and Sliding*, Vol. 155 (ed. S. Childress), pp. 15-33. New York: Springer.

Cotel, A. J. and Webb, P. W. (2015). Living in a turbulent world - a new conceptual framework for the interactions of fish and eddies. *Integr. Comp. Biol.* **55**, 662-672.
Denny, M. W. (1993). *Air and Water: The Biology and Physics of Life's Media*. Princeton, NJ: Princeton University Press.
Drucker, E. G. and Jensen, J. S. (1996). Pectoral fin locomotion in the striped surfperch I. Kinematic effects of swimming speed and body size. *J. Exp. Biol.* **199**, 2235-2242.
Drucker, E. G. and Lauder, G. V. (1999). Locomotor forces on a swimming fish: three-dimensional vortex wake dynamics quantified using digital particle image velocimetry. *J. Exp. Biol.* **202**, 2393-2412.
Drucker, E. G. and Lauder, G. V. (2002). Experimental hydrodynamics of fish locomotion: functional insights from wake visualization. *Integr. Comp. Biol.* **42**, 243-257.
Drucker, E. G., Walker, J. A. and Westneat, M. W. (2005). Mechanics of pectoral fin swimming in fishes. In *Fish Physiology*, Vol. 23 (ed. E. S. Robert and V. L. George), pp. 369-423. New York: Academic Press.
Ellerby, D. J. and Herskin, J. (2013). Swimming flumes as a tool for studying swimming behavior and physiology: current applications and future developments. In *Swimming Physiology of Fish: Towards Using Exercise to Farm a Fit Fish in Sustainable Aquaculture* (ed. A. P. Palstra and J. V. Planas), pp. 345-375. Berlin, Heidelberg: Springer Berlin Heidelberg.
Enders, E. C., Boisclair, D. and Roy, A. G. (2003). The effect of turbulence on the cost of swimming for juvenile Atlantic salmon (*Salmo salar*). *Can. J. Fish. Aquat. Sci.* **60**, 1149-1160.
Fausch, K. D. (1993). Experimental analysis of microhabitat selection by juvenile steelhead (*Oncorhynchus mykiss*) and coho salmon (*O. kisutch*) in a British Columbia stream. *Can. J. Fish. Aquat. Sci.* **50**, 1198-1207.
Fish, F. E. and Lauder, G. V. (2006). Passive and active flow control by swimming fishes and mammals. *Annu. Rev. Fluid Mech.* **38**, 193-224.
Fuchs, H. L. and Gerbi, G. P. (2016). Seascape-level variation in turbulence- and wave-generated hydrodynamic signals experienced by plankton. *Prog. Oceanogr.* **141**, 109-129.
Gaylord, B., Hodin, J. and Ferner, M. C. (2013). Turbulent shear spurs settlement in larval sea urchins. *Proc. Natl Acad. Sci. USA* **110**, 6901-6906.
Gerry, S. P. and Ellerby, D. J. (2014). Resolving shifting patterns of muscle energy use in swimming fish. *PLoS ONE* **9**, e106030.
Guerra, M. and Thomson, J. (2017). Turbulence measurements from 5-beam acoustic Doppler current profilers. *J. Atmos. Ocean. Technol.*
Hove, J., Gordon, M. S., Webb, P. W. and Weihs, D. (2000). A modified Bläzka-type respirometer for the study of swimming metabolism in fishes having deep, laterally compressed bodies or unusual locomotor modes. *J. Fish Biol.* **56**, 1017-1022.
Johansen, J. L., Vaknin, R., Steffensen, J. F. and Domenici, P. (2010). Kinematics and energetic benefits of schooling in the labriform fish, striped surfperch *Embiotoca lateralis*. *Mar. Ecol. Prog. Ser.* **420**, 221-229.
Jones, N. L. and Monismith, S. G. (2008). The influence of whitecapping waves on the vertical structure of turbulence in a shallow estuarine embayment. *J. Phys. Oceanogr.* **38**, 1563-1580.
Kerr, J. R., Manes, C. and Kemp, P. S. (2016). Assessing hydrodynamic space use of brown trout, Salmo trutta, in a complex flow environment: a return to first principles. *J. Exp. Biol.* **219**, 3480-3491.
Korsmeyer, K. E., Steffensen, J. F. and Herskin, J. (2002). Energetics of median and paired fin swimming, body and caudal fin swimming, and gait transition in parrotfish (*Scarus schlegeli*) and triggerfish (*Rhinecanthus aculeatus*). *J. Exp. Biol.* **205**, 1253-1263.
Kundu, P. K., Cohen, I. M. and Dowling, D. R. (2011). *Fluid Mechanics*. Amsterdam: Elsevier Science.
Lacey, R. W. J., Neary, V. S., Liao, J. C., Enders, E. C. and Tritico, H. M. (2012). The IPOS framework: linking fish swimming performance in altered flows from laboratory experiments to rivers. *River Res. Appl.* **28**, 429-443.
Lauder, G. V. and Clark, B. D. (1984). Water flow patterns during prey capture by teleost fishes. *J. Exp. Biol.* **113**, 143-150.
Liao, J. C. (2003). The Karman gait: novel body kinematics of rainbow trout swimming in a vortex street. *J. Exp. Biol.* **206**, 1059-1073.
Liao, J. C. (2004). Neuromuscular control of trout swimming in a vortex street: implications for energy economy during the Karman gait. *J. Exp. Biol.* **207**, 3495-3506.
Liao, J. C. (2006). The role of the lateral line and vision on body kinematics and hydrodynamic preference of rainbow trout in turbulent flow. *J. Exp. Biol.* **209**, 4077-4090.
Liao, J. C. (2007). A review of fish swimming mechanics and behaviour in altered flows. *Philos. Trans. R. Soc. Lond. B Biol. Sci.* **362**, 1973-1993.
Liao, J. C., Beal, D. N., Lauder, G. V. and Triantafyllou, M. S. (2003). Fish exploiting vortices decrease muscle activity. *Science* **302**, 1566.
Lupandin, A. I. (2005). Effect of flow turbulence on swimming speed of fish. *Biol. Bull.* **32**, 461-466.
MacKenzie, B. R. and Kiørboe, T. (1995). Encounter rates and swimming behavior of pause-travel and cruise larval fish predators in calm and turbulent laboratory environments. *Limnol. Oceanogr.* **40**, 1278-1289.
Maia, A., Sheltzer, A. P. and Tytell, E. D. (2015). Streamwise vortices destabilize swimming bluegill sunfish (*Lepomis macrochirus*). *J. Exp. Biol.* **218**, 786-792.
Marras, S., Killen, S. S., Lindström, J., Mckenzie, D. J., Steffensen, J. F. and Domenici, P. (2015). Fish swimming in schools save energy regardless of their spatial position. *Behav. Ecol. Sociobiol.* **69**, 219-226.
McMahon, T. E. and Hartman, G. F. (1989). Influence of cover complexity and current velocity on winter habitat use by juvenile coho salmon (*Oncorhynchus kisutch*). *Can. J. Fish. Aquat. Sci.* **46**, 1551-1557.
Melling, A. (1997). Tracer particles and seeding for particle image velocimetry. *Measurement* **8**, 1406-1416.
Montgomery, J. C., McDonald, F., Baker, C. F., Carton, A. G. and Ling, N. (2003). Sensory integration in the hydrodynamic world of rainbow trout. *Proc. R. Soc. B Biol. Sci.* **270**, S195-S197.
Mussi, M., Summers, A. P. and Domenici, P. (2002). Gait transition speed, pectoral fin-beat frequency and amplitude in Cymatogaster aggregata, Embiotoca lateralis and Damalichthys vacca. *J. Fish Biol.* **61**, 1282-1293.
Newman, J. and Wu, T. (1975). Hydromechanical aspects of fish swimming. In *Swimming and Flying in Nature*, pp. 615-634. Berlin: Springer.
Nikora, V. I., Aberle, J., Biggs, B. J. F., Jowett, I. G. and Sykes, J. R. E. (2003). Effects of fish size, time-to-fatigue and turbulence on swimming performance: a case study of *Galaxias maculatus*. *J. Fish Biol.* **63**, 1365-1382.
Ogilvy, C. S. and DuBois, A. B. (1981). The hydrodynamics of swimming bluefish(Pomatomus saltatrix) in different intensities of turbulence: variation with changes in buoyancy. *J. Exp. Biol.* **92**, 67-85.
Pavlov, D. S., Lupandin, A. I. and Skorobogatov, M. A. (2000). The effects of flow turbulence on the behavior and distribution of fish. *J. Ichthyol.* **40**, S232-S261.
Pope, S. B. (2000). *Turbulent Flows*. Cambridge, UK: Cambridge University Press.
Przybilla, A., Kunze, S., Rudert, A., Bleckmann, H. and Brücker, C. (2010). Entraining in trout: a behavioural and hydrodynamic analysis. *J. Exp. Biol.* **213**, 2976-2986.
Puckett, K. J. and Dill, L. M. (1984). The energetics of feeding territoriality in juvenile coho salmon (*Oncorhynchus kisutch*). *Behaviour* **92**, 97-110.
Raffel, M., Willert, C. E., Wereley, S. T. and Kompenhans, J. (2007). *Particle Image Velocimetry: A Practical Guide*. Berlin: Springer-Verlag.
Roche, D. G., Taylor, M. K., Binning, S. A., Johansen, J. L., Domenici, P. and Steffensen, J. F. (2014). Unsteady flow affects swimming energetics in a labriform fish (*Cymatogaster aggregata*). *J. Exp. Biol.* **217**, 414-422.
Seo, Y. (2013). Effect of hydraulic diameter of flow straighteners on turbulence intensity in square wind tunnel. *HVAC&R Res.* **19**, 141-147.
Shuler, S. W., Nehring, R. B. and Fausch, K. D. (1994). Diel habitat selection by brown trout in the Rio Grande river, Colorado, after placement of boulder structures. *North Am. J. Fish Manag.* **14**, 99-111.
Singh, S. P. and Mittal, S. (2005). Flow past a cylinder: shear layer instability and drag crisis. *Int. J. Numer. Methods Fluids* **47**, 75-98.
Smith, M. R., Hilton, D. K. and Sciver, S. W. V. (1999). Observed drag crisis on a sphere in flowing HeI and HeII. *Phys. Fluids* **11**, 751-753.
Standen, E. M., Hinch, S. G. and Rand, P. S. (2004). Influence of river speed on path selection by migrating adult sockeye salmon (Oncorhynchus nerka). *Can. J. Fish. Aquat. Sci.* **61**, 905-912.
Steffensen, J. F. (1989). Some errors in respirometry of aquatic breathers: how to avoid and correct for them. *Fish Physiol. Biochem.* **6**, 49-59.
Steffensen, J. F., Johansen, K. and Bushnell, P. G. (1984). An automated swimming respirometer. *Comp. Biochem. Physiol. A Physiol.* **79**, 437-440.
Sutterlin, A. M. and Waddy, S. (1975). Possible role of the posterior lateral line in obstacle entrainment by brook trout (*Salvelinus fontinalis*). *J. Fish. Res. Board Can.* **32**, 2441-2446.
Svendsen, J. C., Tudorache, C., Jordan, A. D., Steffensen, J. F., Aarestrup, K. and Domenici, P. (2010). Partition of aerobic and anaerobic swimming costs related to gait transitions in a labriform swimmer. *J. Exp. Biol.* **213**, 2177-2183.
Svendsen, M. B. S., Bushnell, P. G. and Steffensen, J. F. (2016). Design and setup of intermittent-flow respirometry system for aquatic organisms. *J. Fish Biol.* **88**, 26-50.
Taguchi, M. and Liao, J. C. (2011). Rainbow trout consume less oxygen in turbulence: the energetics of swimming behaviors at different speeds. *J. Exp. Biol.* **214**, 1428-1436.
Tennekes, H. and Lumley, J. L. (1972). *A First Course in Turbulence*. Cambridge, MA: MIT Press.
Tritico, H. M. and Cotel, A. J. (2010). The effects of turbulent eddies on the stability and critical swimming speed of creek chub (Semotilus atromaculatus). *J. Exp. Biol.* **213**, 2284-2293.
Vetriselvan, M. and Munuswamy, N. (2011). Morphological and molecular characterization of various Artemia strains from tropical saltpans in South East Coast of India. *J. Am. Sci.* **7**, 689-695.
Vogel, S. (1994). *Life in Moving Fluids: The Physical Biology of Flow*. Princeton, New Jersey: Princeton University Press.
Weatherley, A. H., Rogers, S. C., Pinock, D. G. and Patch, J. R. (1982). Oxygen consumption of active rainbow trout, *Salmo gairdneri* Richardson, derived from electromyograms obtained by radiotelemetry. *J. Fish Biol.* **20**, 479-489.
Webb, P. W. (1973). Kinematics of pectoral fin propulsion in *Cymatogaster Aggregata*. *J. Exp. Biol.* **59**, 697-710.

Webb, P. W. (1975). Hydrodynamics and energetics of fish propulsion. *Bull. Fish. Res. Board Can.* **190**, 1-158.
Webb, P. W. (1984). Body form, locomotion and foraging in aquatic vertebrates. *Am. Zool.* **24**, 107-120.
Webb, P. W. (1991). Composition and mechanics of routine swimming of rainbow trout, *Oncorhynchus mykiss*. *Can. J. Fish. Aquat. Sci.* **48**, 583-590.
Webb, P. W. (1998). Entrainment by river chub *Nocomis micropogon* and smallmouth bass *Micropterus dolomieu* on cylinders. *J. Exp. Biol.* **201**, 2403-2412.
Webb, P. W. and Cotel, A. J. (2010). Turbulence: does vorticity affect the structure and shape of body and fin propulsors? *Integr. Comp. Biol.* **50**, 1155-1166.
Webb, P. W., Cotel, A. J. and Meadows, L. A. (2010). Waves and eddies: effects on fish behavior and habitat distribution. In *Fish Locomotion: An Eco-ethological Perspective* (ed. P. Domenici and B. G. Kapoor), pp. 1-39. Boca Raton, FL: CRC Press.
Wichert, S., Fokianos, K. and Strimmer, K. (2004). Identifying periodically expressed transcripts in microarray time series data. *Bioinformatics* **20**, 5-20.
Wood, S. (2017). *Generalized Additive Models: An Introduction with R*. Boca Raton, FL: Chapman and Hall/CRC.
Zuur, A. F., Ieno, E. N. and Elphick, C. S. (2010). A protocol for data exploration to avoid common statistical problems. *Methods Ecol. Evol.* **1**, 3-14.

Table S1. Metrics used to quantify flow variability. The angle-bracket operator is used to denote the spatiotemporal average of a quantity such that $\langle \boldsymbol{U} \rangle = \int_0^T \int_0^L \int_0^H \boldsymbol{U} \cdot \boldsymbol{dh} \cdot \boldsymbol{dl} \cdot \boldsymbol{dt}$ where T is the time period of measurement, L is the length of the working section, and H is the height of the working section. The overbar operator denotes a time-average only. Note that because our PIV measurement window is two-dimensional, we may only calculate the y- (out-of-plane) component of vorticity, $\boldsymbol{\omega_y}$. Each turbulence parameter or lengthscale was calculated using the entire PIV measurement region, excluding fluid within 2cm of the walls and grids to avoid boundary layer effects. Quantities were averaged over each image frame and then bootstrapped in time with 1000 replicates to determine 95% Confidence Interval (CI). Note that the flow velocity $= \bar{U} + u'$, where $\bar{U}$ is the time-averaged component and u' is the fluctuating component.

Parameter	Definition	Qualitative measure
Turbulent velocity scale [$m\ s^{-1}$]	$u_T \equiv \sqrt{\frac{1}{3}(\langle u'^2 \rangle + 2\langle w'^2 \rangle)}$	Average fluctuating velocity experienced at any point
Turbulent Kinetic Energy (TKE) [$m^2\ s^{-3}$]	$q^2 \equiv \frac{3}{2} u_T^2$	Average energy of flow
Turbulence intensity (TI) [ ]	$TI \equiv \frac{u_T}{\langle U \rangle}$	"Percent unsteadiness" of flow; bulk measure describing ratio of "disturbance to damping" (e.g., see Cotel and Webb, 2012)
Bulk Enstrophy [s^{-2}]	$\langle \omega_y^2 \rangle \equiv \langle \left(\frac{\partial w}{\partial x} - \frac{\partial u}{\partial z} \right)^2 \rangle$	Average amount of rotation in flow
Dissipation rate [$m^2 s^{-2}$]	$\varepsilon = 4\nu \langle \overline{\left(\frac{\partial u}{\partial x} \right)^2} + \overline{\left(\frac{\partial w}{\partial z} \right)^2} + \overline{\frac{\partial u}{\partial x} \frac{\partial w}{\partial z}} + \frac{3}{4} \overline{\left(\frac{\partial u}{\partial x} + \frac{\partial w}{\partial z} \right)^2} \rangle$	Rate of energy dissipation at small scales, equal to the rate of energy transfer at intermediate scales (estimated for 2D volume, based on de Jong et al., 2009).

Streamwise integral lengthscale $[m]$	$L_{xx} = \int_0^\infty \frac{\langle u'(x+r) \cdot u'(x) \rangle}{\langle u'(x) \cdot u'(x) \rangle} dr$	Average streamwise extent of turbulent eddies (Pope 2000)
Vertical integral lengthscale $[m]$	$L_{zz} = \int_0^\infty \frac{\langle w'(z+r) \cdot w'(y) \rangle}{\langle w'(z) \cdot w'(z) \rangle} dr$	Average streamwise extent of turbulent eddies (Pope 2000)
Taylor microscale	$\lambda = \sqrt{\frac{15\nu}{\varepsilon}}$	Average distance between stagnation points in the flow (Pope 2000)
Kolmogorov microscale	$\eta = \left(\frac{\nu^3}{\varepsilon}\right)^{\frac{1}{4}}$	Lengthscale at which kinetic energy begins to dissipate into heat (Pope 2000)

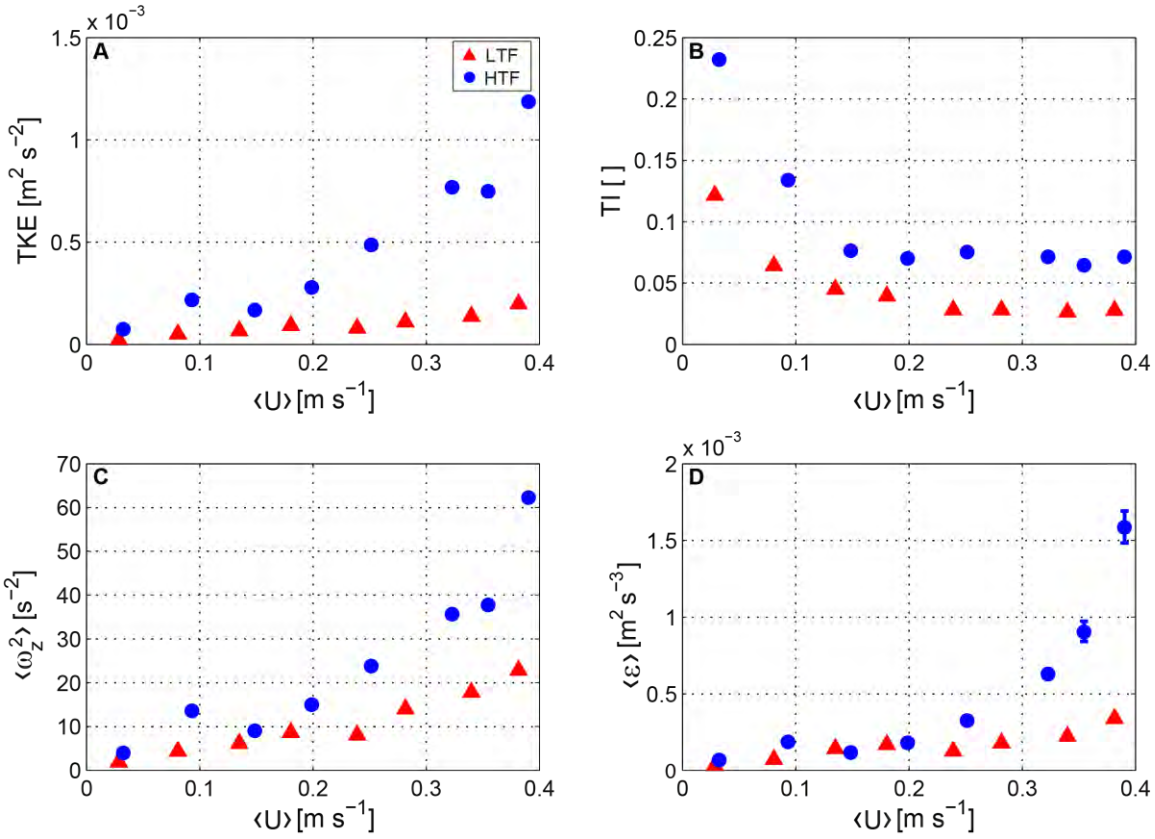

Fig. S1. Particle Image Velocimetry (PIV) reveals significantly different flow regimes in low- (LTF) and high-turbulence flow (HTF) conditions set up in the swimming respirometer across a range of mean flow speeds. (A) Turbulent kinetic energy ($m^2 s^{-2}$), (B) turbulence intensity (dimensionless), (C) enstrophy (s^{-2}) and (D) turbulent dissipation rate ($m^2 s^{-3}$) averaged over the measurement window in LTF and HTF, over the full range of mean streamwise velocities ($m s^{-1}$) experienced by swimming shiner perch. Quantities were calculated from velocity fields measured using PIV. Error bars represent 95% confidence intervals obtained by bootstrapping with 1000 replicates. Some error bars are too small to appear on the figure.

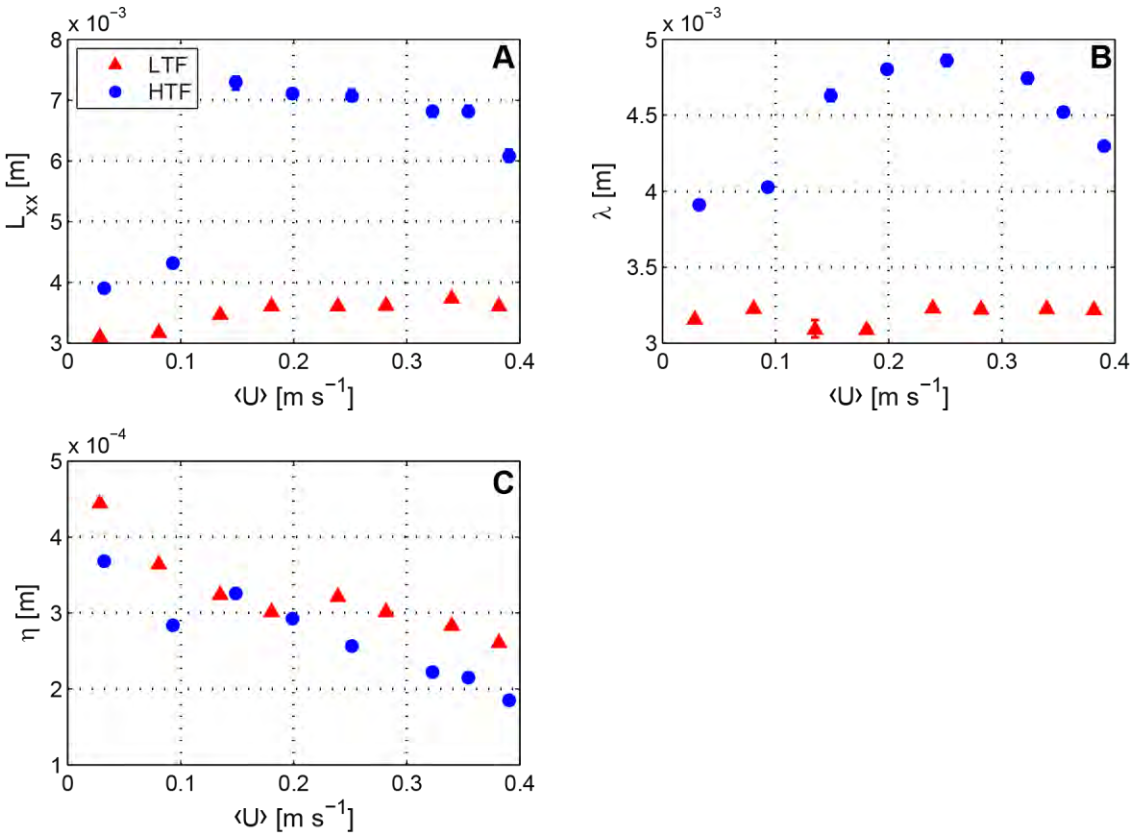

Fig. S2. Turbulent lengthscales in high- (HTF) and low-turbulence flow (LTF) regimes in the swimming respirometer at different flow speeds. Streamwise integral lengthscale L_{xx} (A), Taylor microscale $\lambda\lambda$ (B), and Kolmogorov microscale η (C). Error bars represent 95% confidence intervals obtained via bootstrapping with 1000 replicates. Some error bars are too small to appear in the figure.

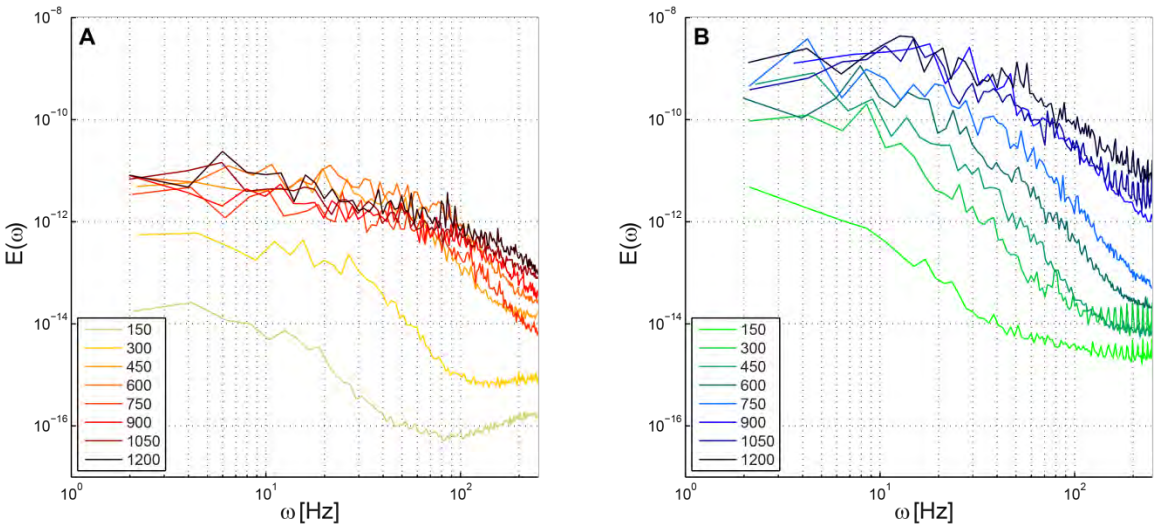

Fig. S3. Frequency spectra of both LTF (A) and HTF (B). Legend shows motor rpm, which was used during calibration in lieu of the later calculated mean flow speeds. Equivalent motor rpm corresponds to approximately equivalent mean flow speed.

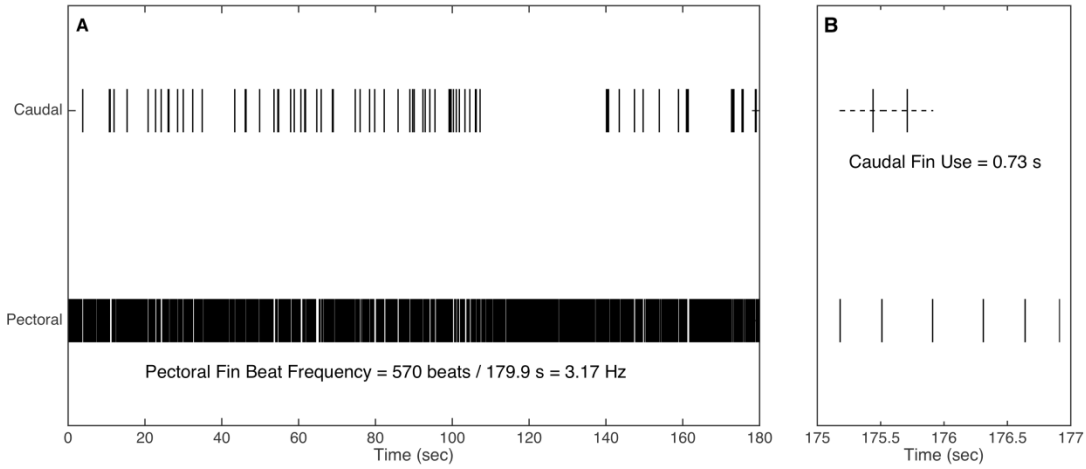

Fig. S4. Individual caudal and pectoral fin beats for over (A) one 180 s sampling period, showing how pectoral fin beat frequency is calculated; and (B) the last few seconds of the same sampling period, showing how caudal fin use (dashed horizontal line) is calculated.

Script 1. This R Markdown document details the statistical approach for the paper van der Hoop et al. 201X "Turbulent flow reduces oxygen consumption in the labriform swimming shiner perch, Cymatogaster aggregata"

The data represent mean oxygen consumption rates (MO2; mg O_2/kg/h) from three measurements at each speed (repetition number) of increments from 0.5 Body Lengths (BL) per second [BL/s] up to a maximum swimming speed, for different Fish that swam each in High ("T") and Low ("L") turbulence flow conditions in a respirometer. Bacterial MO2 (mg O_2/h) for each trial are subtracted from the measured MO2.

```
## 1. Data handling

# load data
library(readxl)
fish <- read_xlsx("FHL_FishVO2_allreps.xlsx")

# make the things that need to be factors factors
fish$Fish <- as.factor(fish$Fish)
fish$Flow <- as.factor(fish$Flow)
fish$Rep <- as.factor(fish$Rep)

## 2. Model Fitting
library(nlme)

# We want to fit something of the form
#  O2 ~ a + b*Speed^c
# estimate a,b,c and have a random effect for fish
# each a,b,c has two levels, one for each treatment (Low-Turbulence and High-Turbulence)

# NOTES:
# - formula is NOT a standard R formula
# - fixed specifies the form for the fixed effects (the a,b,c parameters)
# - random says what the random effects are (random intercept for a)
modr <- nlme(VO2minBac~a+b*Speed^c,
             fixed = a+b+c~Flow,
             random = a+b+c~1|Fish,
             start=c(168.7038472,0, 6,0, 2.2036793, 0),
             data=fish)

# Check model summary
summary(modr)
```

```
## Nonlinear mixed-effects model fit by maximum likelihood
##   Model: VO2minBac ~ a + b * Speed^c
##  Data: fish
##        AIC      BIC    logLik
##   3866.919 3918.209 -1920.459
##
## Random effects:
##  Formula: list(a ~ 1, b ~ 1, c ~ 1)
```

```
##  Level: Fish
##  Structure: General positive-definite, Log-Cholesky parametrization
##               StdDev       Corr
## a.(Intercept) 1.910258e+01 a.(In) b.(In)
## b.(Intercept) 7.802433e-08 -0.138
## c.(Intercept) 3.073572e-01  0.210 -0.658
## Residual      3.442769e+01
##
## Fixed effects: a + b + c ~ Flow
##                    Value Std.Error  DF   t-value p-value
## a.(Intercept) 167.19921  8.246068 369 20.276233  0.0000
## a.FlowT       -10.53301  6.418565 369 -1.641023  0.1016
## b.(Intercept)   4.99231  1.157339 369  4.313611  0.0000
## b.FlowT         1.42991  2.435864 369  0.587026  0.5575
## c.(Intercept)   2.89096  0.196620 369 14.703291  0.0000
## c.FlowT        -0.66851  0.287043 369 -2.328942  0.0204
##  Correlation:
##               a.(In) a.FlwT b.(In) b.FlwT c.(In)
## a.FlowT       -0.340
## b.(Intercept) -0.411  0.370
## b.FlowT        0.108 -0.672 -0.270
## c.(Intercept)  0.413 -0.275 -0.825  0.220
## c.FlowT       -0.142  0.623  0.388 -0.981 -0.324
##
## Standardized Within-Group Residuals:
##        Min         Q1        Med         Q3        Max
## -2.4264658 -0.5157803 -0.1067824  0.4336127  5.5249318
##
## Number of Observations: 382
## Number of Groups: 8
```

```
## Number of Observations: 382
## Number of Groups: 8
```

```r
# plot observed vs predicted
plot(fish$VO2minBac, predict(modr),
     asp=1,
     xlab="Observed VO2minBac", ylab="Predicted VO2minBac")
abline(a=0,b=1, col="blue", lty=2)
```

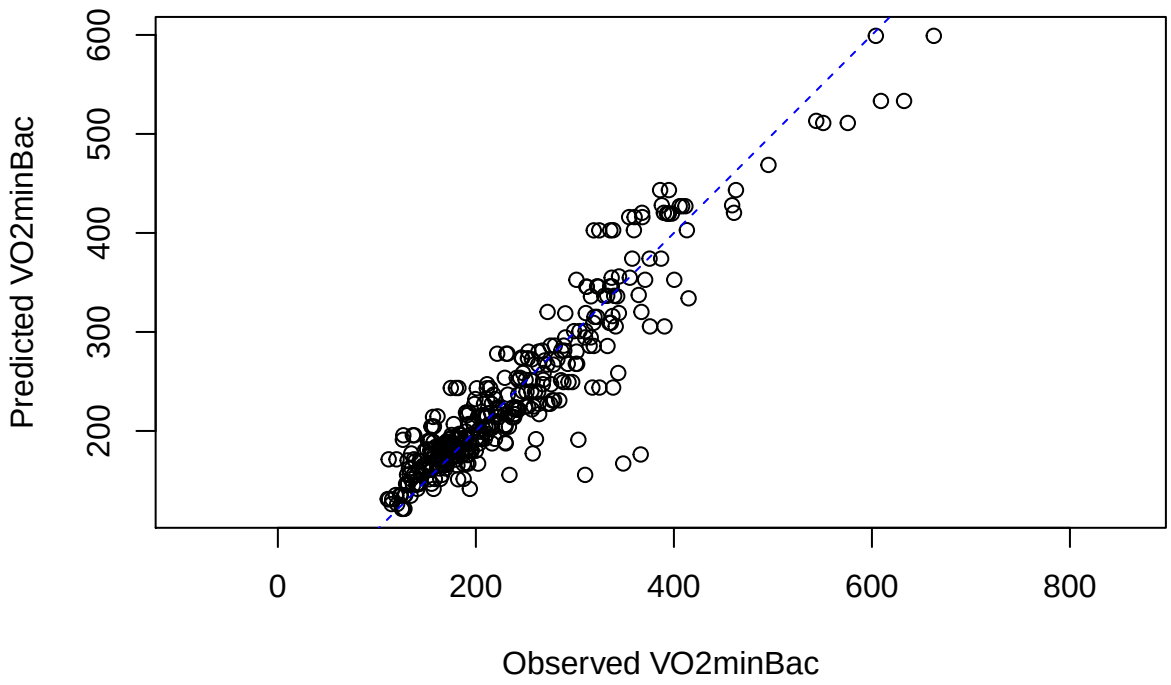


```
# same but average over repetitions
# (a bit cleaner)
plot(aggregate(fish$VO2minBac, list(fish$Speed, fish$Flow, fish$Fish), mean)$x,
     aggregate(predict(modr), list(fish$Speed, fish$Flow, fish$Fish), mean)$x,
     main="modr - aggregated observed vs predicted",
     asp=1,
     xlab="Observed VO2minBac", ylab="Predicted VO2minBac")
abline(a=0,b=1, col="blue", lty=2)
```

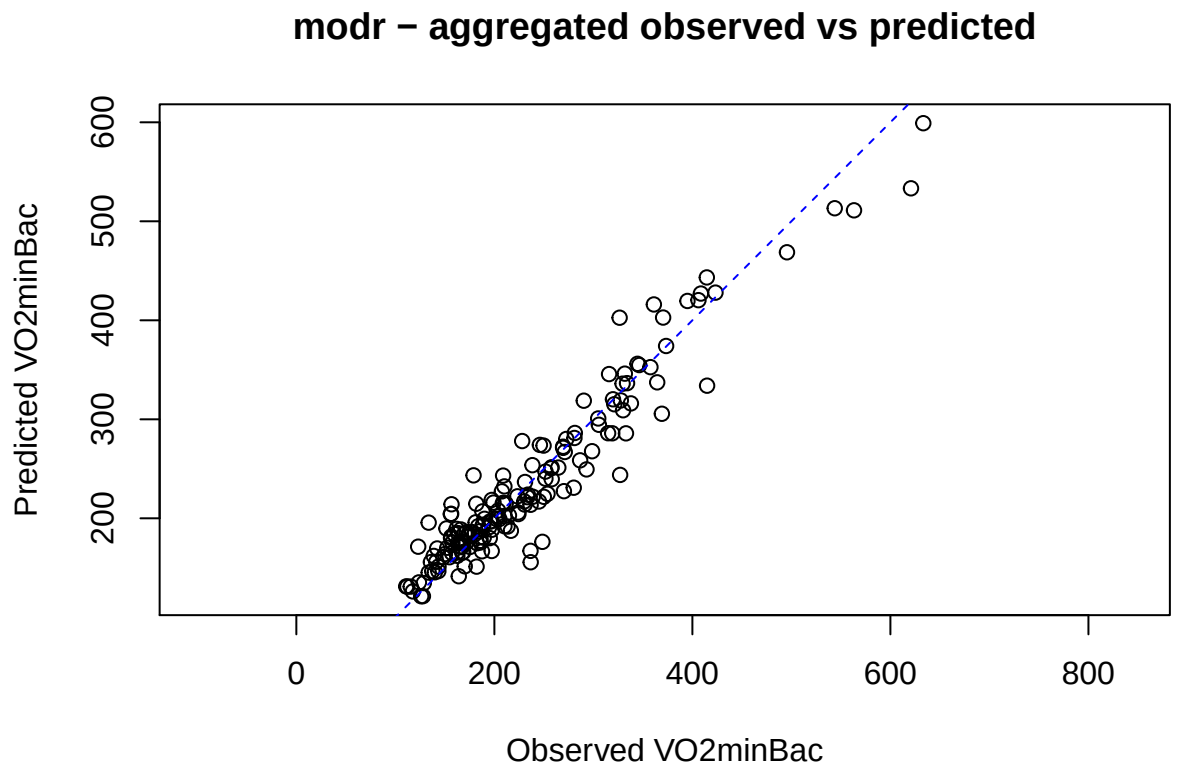


```
## 3. Model checking

# per fish residuals - this looks okay, no major variations
bp_dat <- data.frame(resids = residuals(modr),
                     Fish   = fish$Fish)
boxplot(resids~Fish, bp_dat, varwidth=TRUE, ylim=c(-100, 200))
```

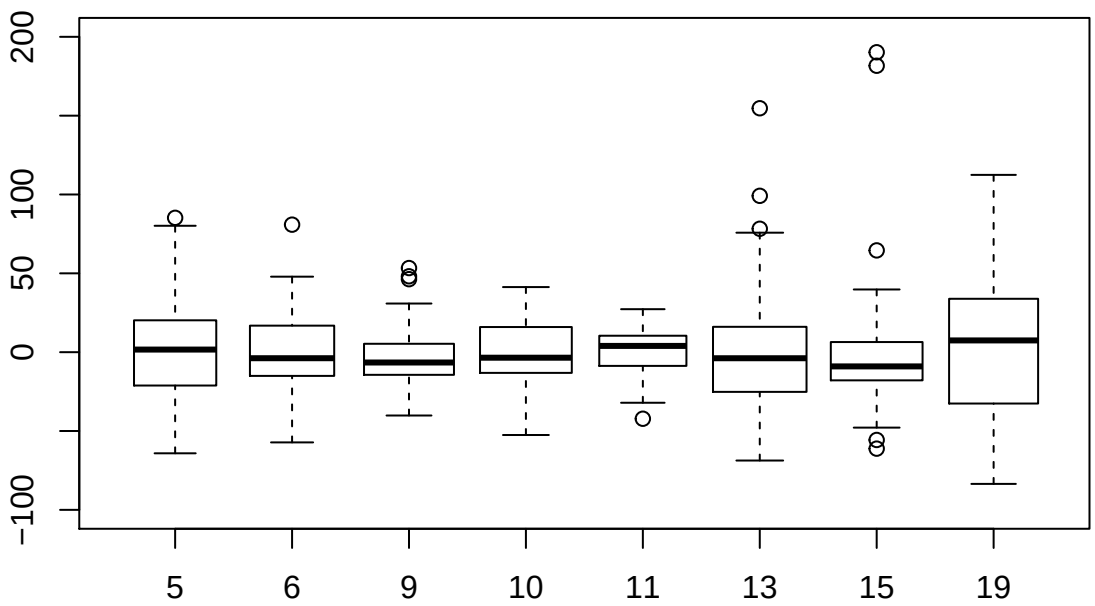


```
# residuals by Speed
# - these look okay too, maybe some increase in variance at higher speeds
dat <- data.frame(residuals = residuals(modr),
#                 Speed     = cut(fish$Speed, seq(0.25,4.75,0.5)))
```

```
                    Speed     = cut(fish$Speed, c(seq(0.25,3.75,0.5), 4.75)))
boxplot(residuals~Speed, dat, varwidth=TRUE, ylim=c(-100, 200))
```

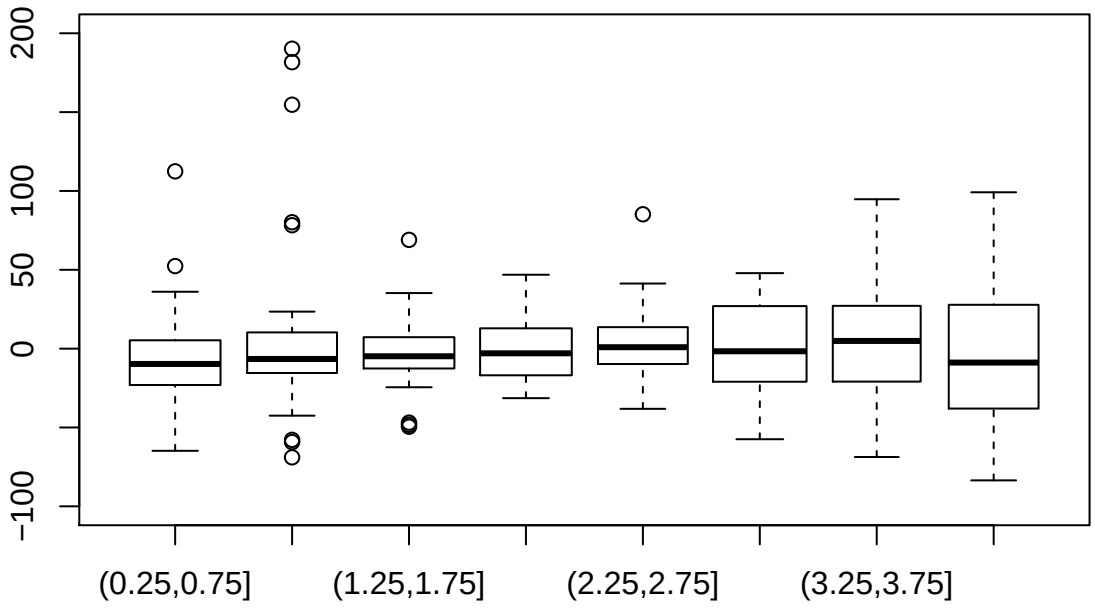


```
# predictions vs. residuals
plot(modr)
```

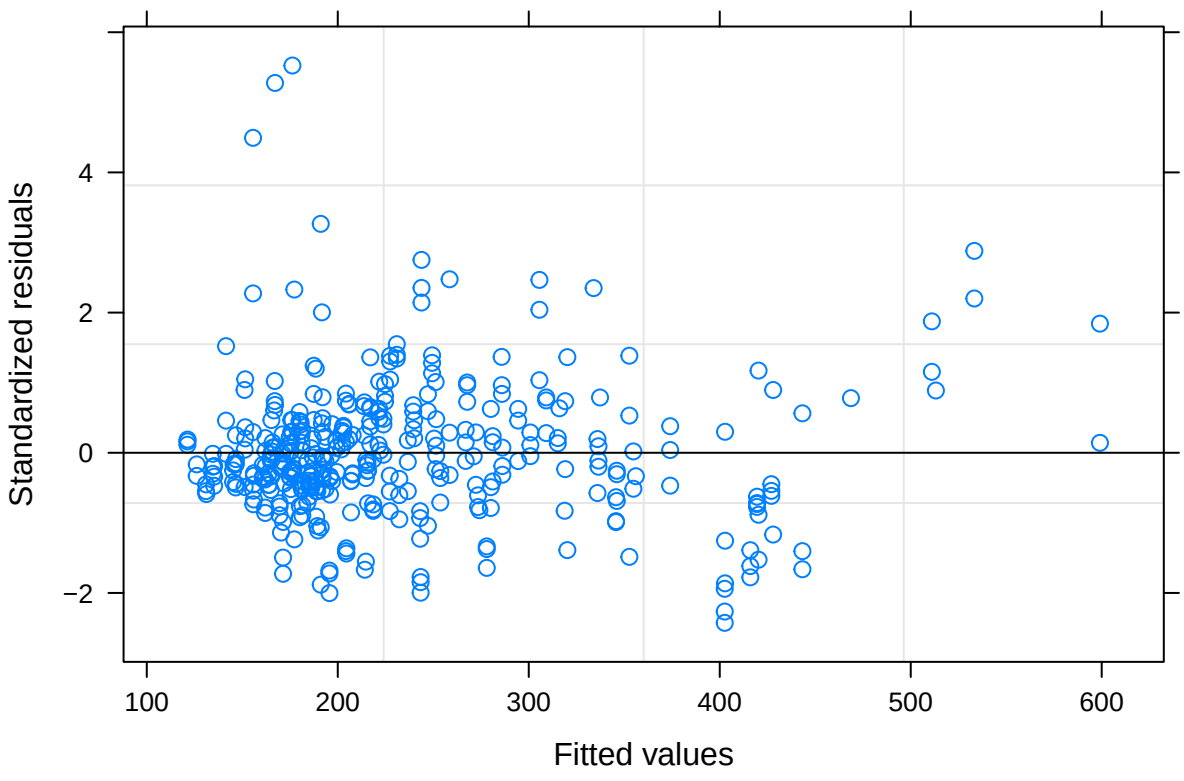


```
plot(modr, resid(.) ~ Speed)
```

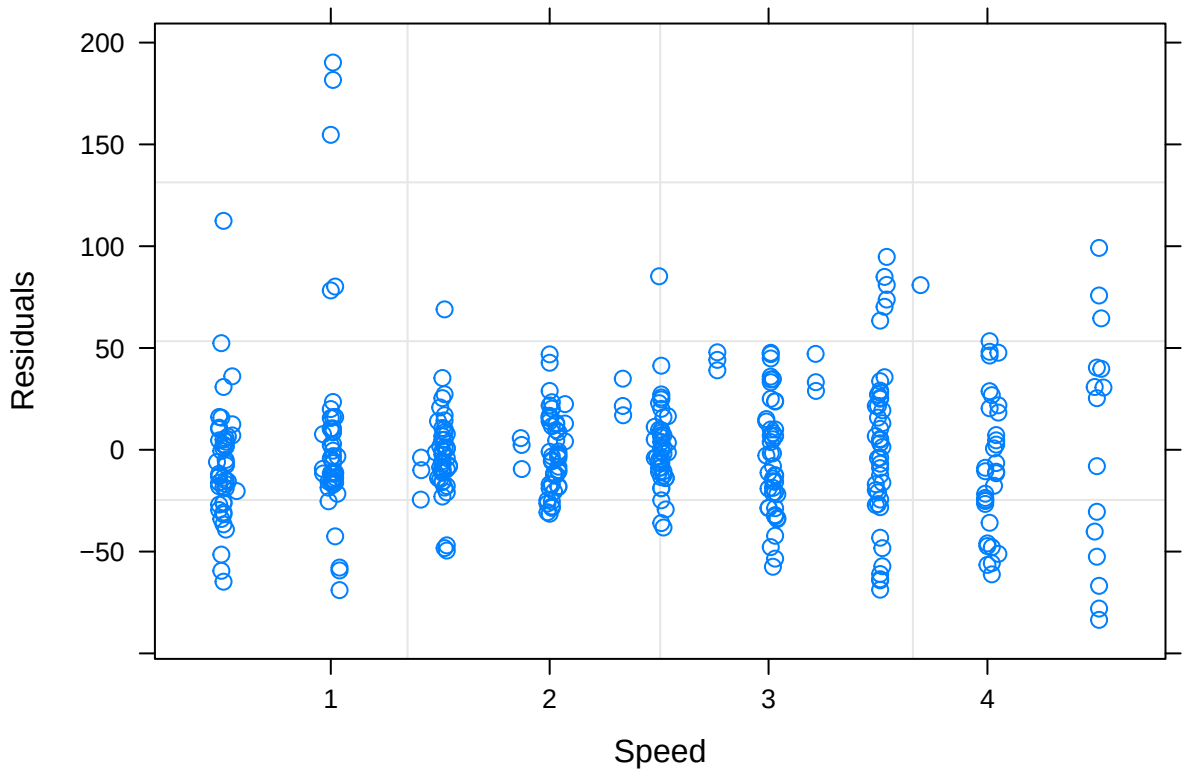


```
# what aout a q-q plot of the residuals
# - not perfect: looks like we aren't doing such a good job in the tails?
qqnorm(modr, abline=c(0,1))
```

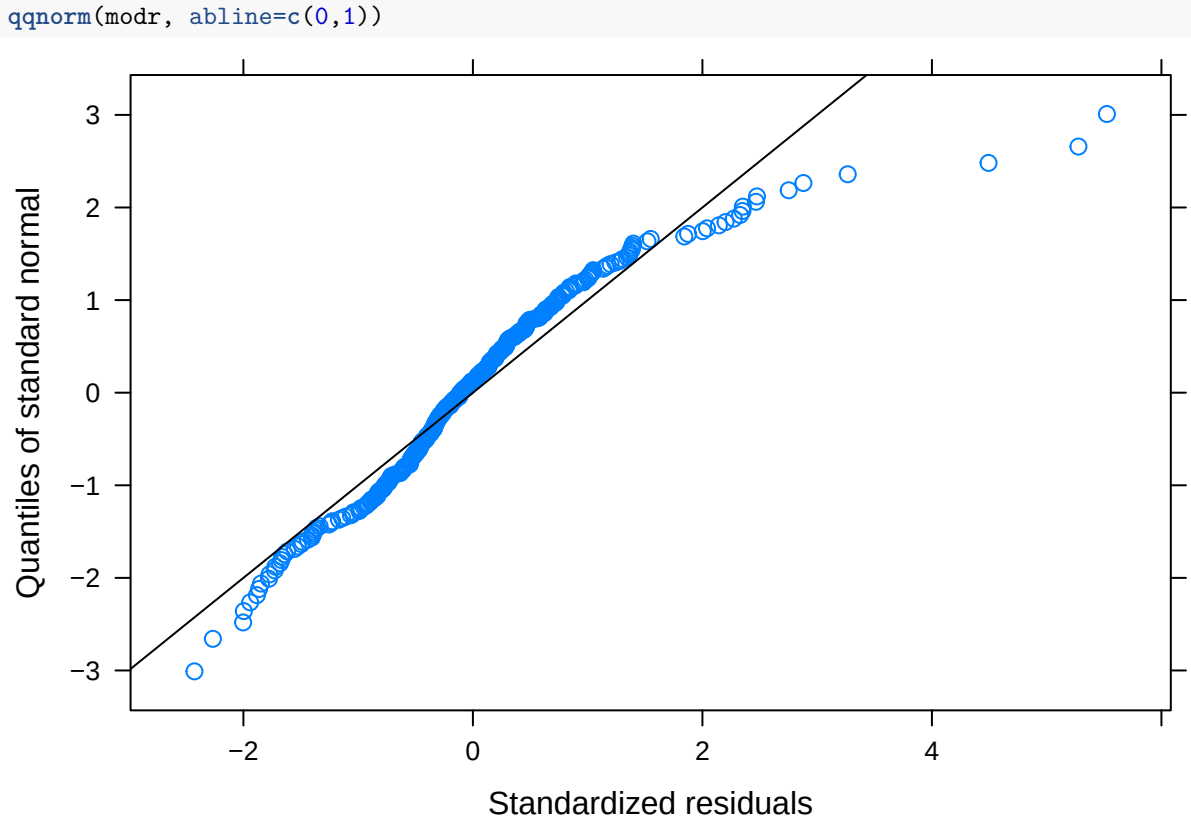

```
# q-q of the random effects - they should be normal
qqnorm(modr, ~ranef(.))
```

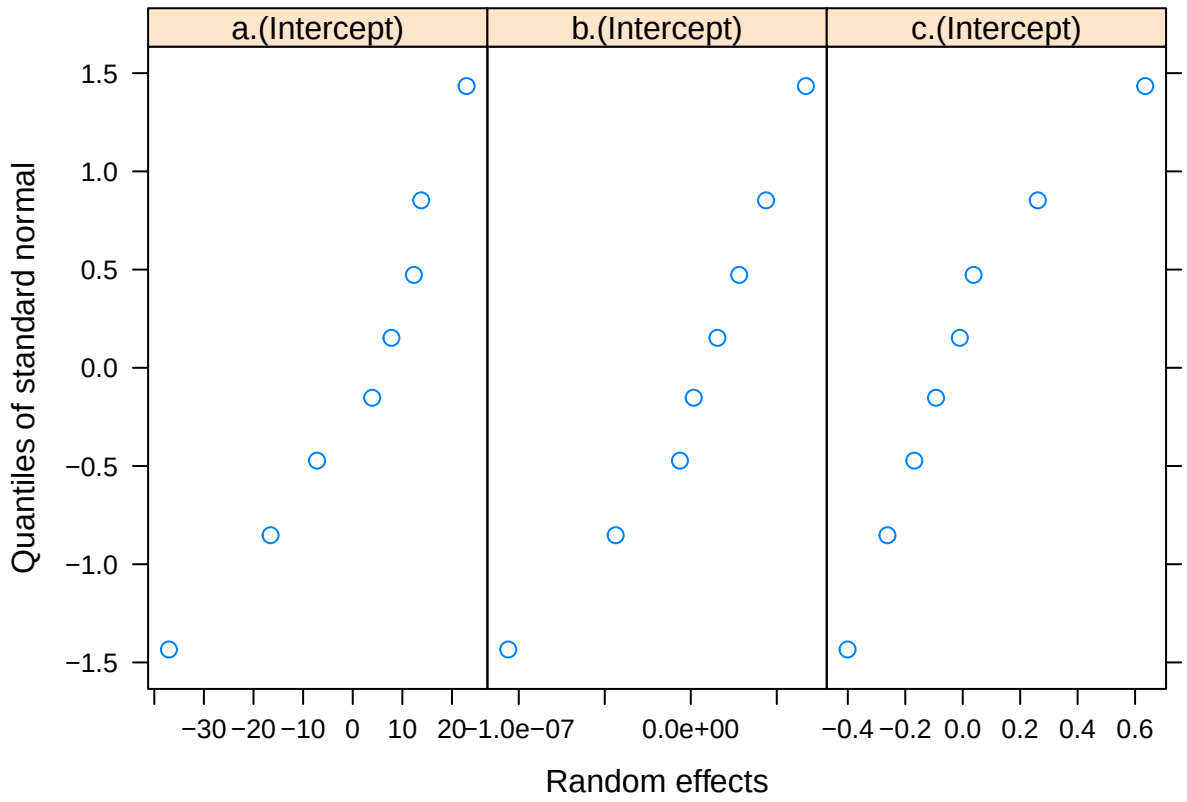


```
## 4. prediction plots
library(ggplot2)

# plot predictions per Fish
# make prediction grid, then predict
preddat <- expand.grid(Speed = seq(0.5, 4.5, by=0.1),
                       Flow  = c("L", "T"), # L = LTF, T = HTF
                       Fish  = unique(fish$Fish))
plotty <- predict(modr, preddat, level=1)
plotty <- cbind(preddat, VO2minBac=plotty)

p <- ggplot(plotty, aes(x=Speed, y=VO2minBac, group=Flow, colour=Flow)) +
  geom_line(size=0.75, linetype=2) +
  geom_point(data=fish) +
  facet_wrap(~Fish, nrow=2) +
  theme_minimal() +
  # scale_colour_brewer(type="qual")
  scale_color_manual(values=c('blue', 'red')) +
  scale_shape_manual(values=c(17, 16))+
  labs(x="Speed (BL/s)", y = expression("Oxygen Consumption Rate, MO"[2]* " ("*mg.kg^{-1}*.h^{-1}*")"), colour="Condition")
print(p)
```

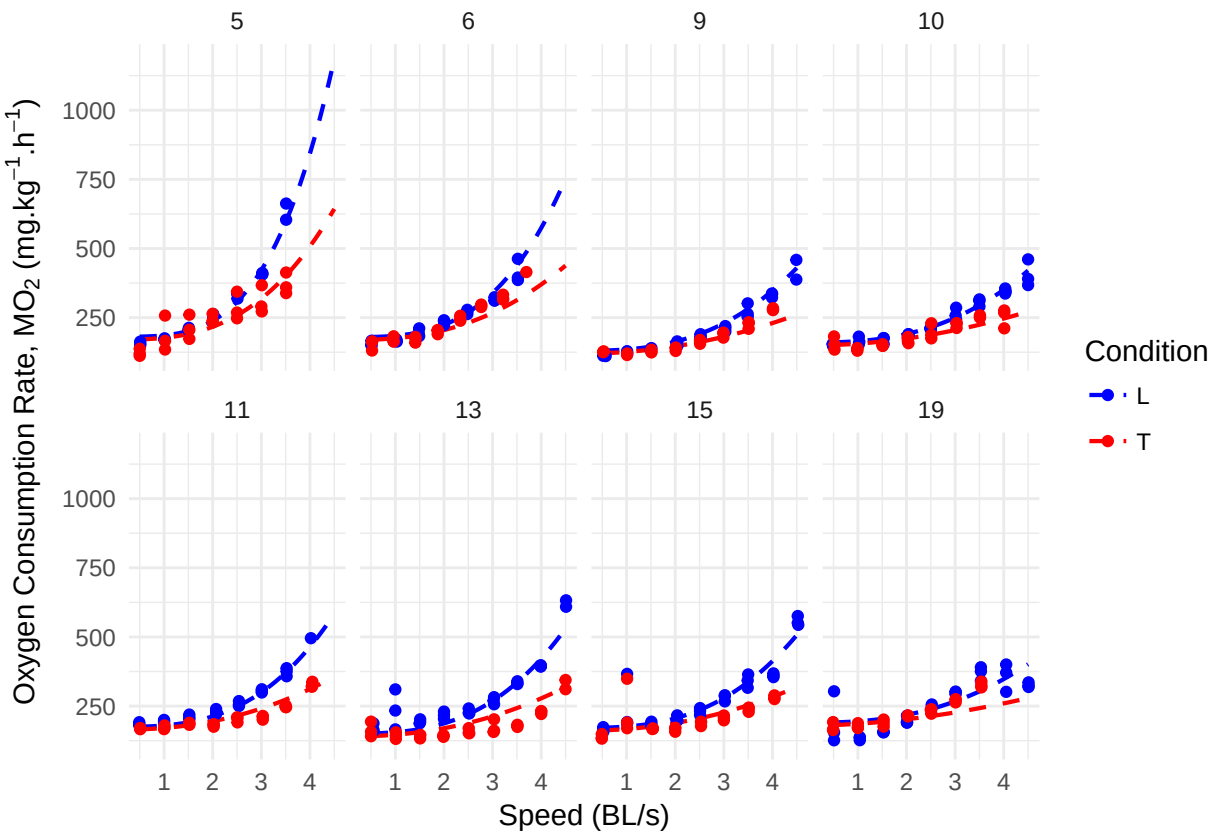


```
# plot predictions averaged over Fish
# make prediction grid, then predict
preddat <- expand.grid(Speed = seq(0.5, 4.5, by=0.1),
                       Flow  =  c("L", "T"))
plotty <- predict(modr, preddat, level=0)
plotty <- cbind(preddat, VO2minBac=plotty)

p <- ggplot(plotty, aes(x=Speed, y=VO2minBac, group=Flow, colour=Flow)) +
  geom_line(size=0.75, linetype=2) +
  geom_point(data=fish, size=1.5, aes(shape=Flow)) +
  theme_minimal() +
  scale_colour_manual(values=c("red", "blue")) +
  scale_shape_manual(values=c(17, 16))+
  labs(x="Speed (BL/s)", y = expression("Oxygen Consumption Rate, MO"[2]* " ("*mg.kg^{-1}*.h^{-1}*")"), colour="Condition")
print(p)
```

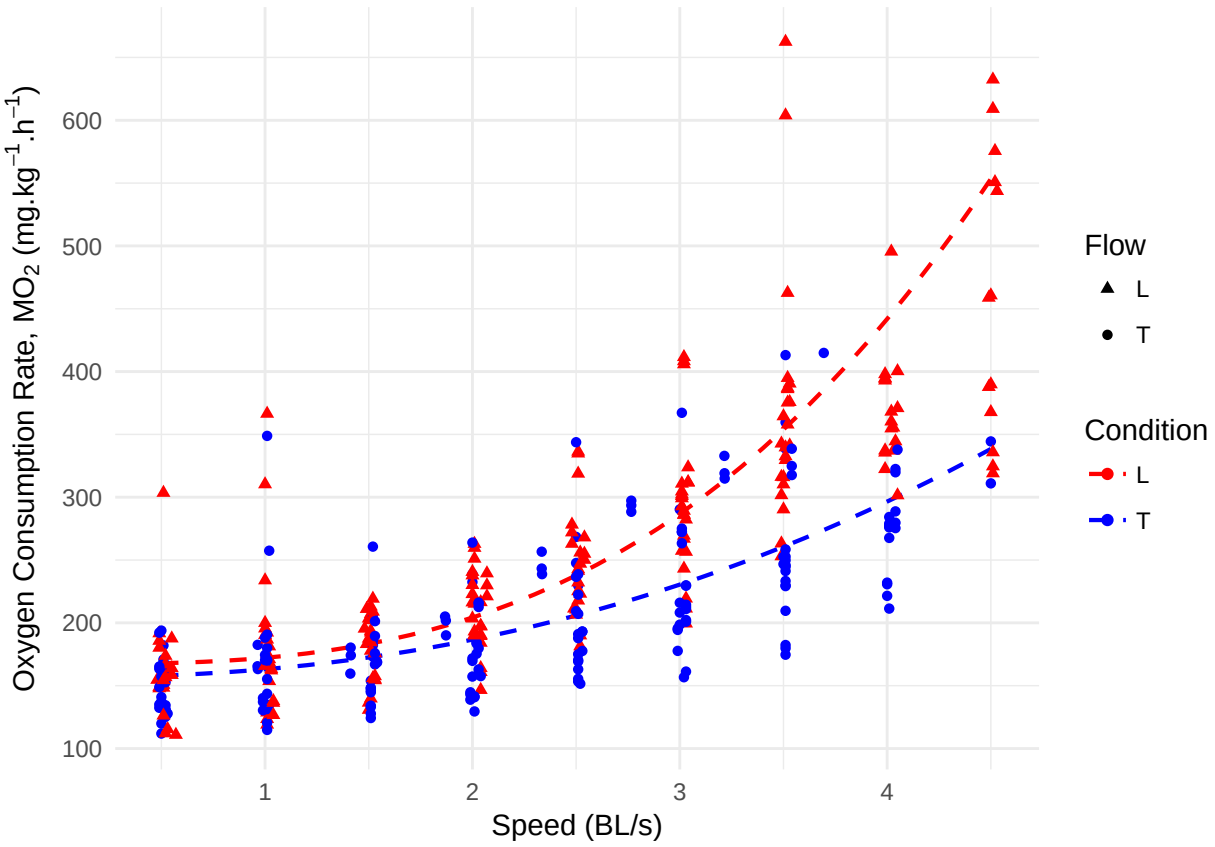


```
# Paired data for comparison of MO2 between LTF and HTF at each speed
paireddata <- read_xlsx("/Users/julievanderhoop/Documents/Courses/Biol533_FishSwimming_FHL/VO2.xlsx", sheet = 11)  # read 11th sheet

t05 <- t.test(paireddata$L[which(paireddata$Speed==0.5)],paireddata$T[which(paireddata$Speed==0.5)],paired = TRUE)
t1 <- t.test(paireddata$L[which(paireddata$Speed==1)],paireddata$T[which(paireddata$Speed==1)],paired = TRUE)
t15 <- t.test(paireddata$L[which(paireddata$Speed==1.5)],paireddata$T[which(paireddata$Speed==1.5)],paired = TRUE)
t2 <- t.test(paireddata$L[which(paireddata$Speed==2.0)],paireddata$T[which(paireddata$Speed==2.0)],paired = TRUE)
t25 <- t.test(paireddata$L[which(paireddata$Speed==2.5)],paireddata$T[which(paireddata$Speed==2.5)],paired = TRUE)
t3 <- t.test(paireddata$L[which(paireddata$Speed==3.0)],paireddata$T[which(paireddata$Speed==3.0)],paired = TRUE)
t35 <- t.test(paireddata$L[which(paireddata$Speed==3.5)],paireddata$T[which(paireddata$Speed==3.5)],paired = TRUE)
t4 <- t.test(paireddata$L[which(paireddata$Speed==4.0)],paireddata$T[which(paireddata$Speed==4.0)],paired = TRUE)

pvals <- c(t05$p.value,t1$p.value,t15$p.value,t2$p.value,t25$p.value,t3$p.value,t35$p.value,t4$p.value)
BH <- p.adjust(pvals,"BH")
```

To assess how MO2 changed with fin beat frequency, we fitted a generalized additive model (Wood, 2017) to the MO2, using pectoral or caudal fin beat (Hz) as separate explanatory variables. We used factor-smooth interactions (Baayen et al., 2016) to fit two levels of a smoothed function of measured beat frequency, one for each flow condition. Such terms fit the base level of the factor as a smooth, then model deviations from that smooth for the other level, thus information is shared between the models while allowing for a flexible relationship that makes no assumptions about functional form. Fish ID was included as a random effect. Models were fitted by restricted maximum likelihood.

```
hz <- read.csv("/Users/julievanderhoop/Documents/Courses/Biol533_FishSwimming_FHL/FishVO2Hz.csv")

# make codes for the speeds
hz$speedcode <- "H"
hz$speedcode[hz$speed == 0.5] <- "L"
```

```
hz$speedcode[hz$speed == 1.5] <- "M"
# speeds set at 0.5, 1.5 and then the max speed achieved for both LTF and HTF

library(ggplot2)

# quick visualisation
p <- ggplot(hz) +
  #geom_point(aes(x=speed, y=VO2minBac, colour=cond)) +
  geom_point(aes(x=PecHz, y=VO2minBac, colour=cond)) +
  theme_minimal() +
  scale_shape_manual(values=c(16, 17)) +
  scale_color_manual(values=c('red', 'blue')) +
  labs(x="Pectoral Fin Beat Frequency (Hz)", y = expression("Oxygen Consumption Rate, MO"[2]* " ("*mg.kg^{-1}*.h^{-1}*")"), colour="Condition")+
  facet_wrap(~Fish)
print(p)
```

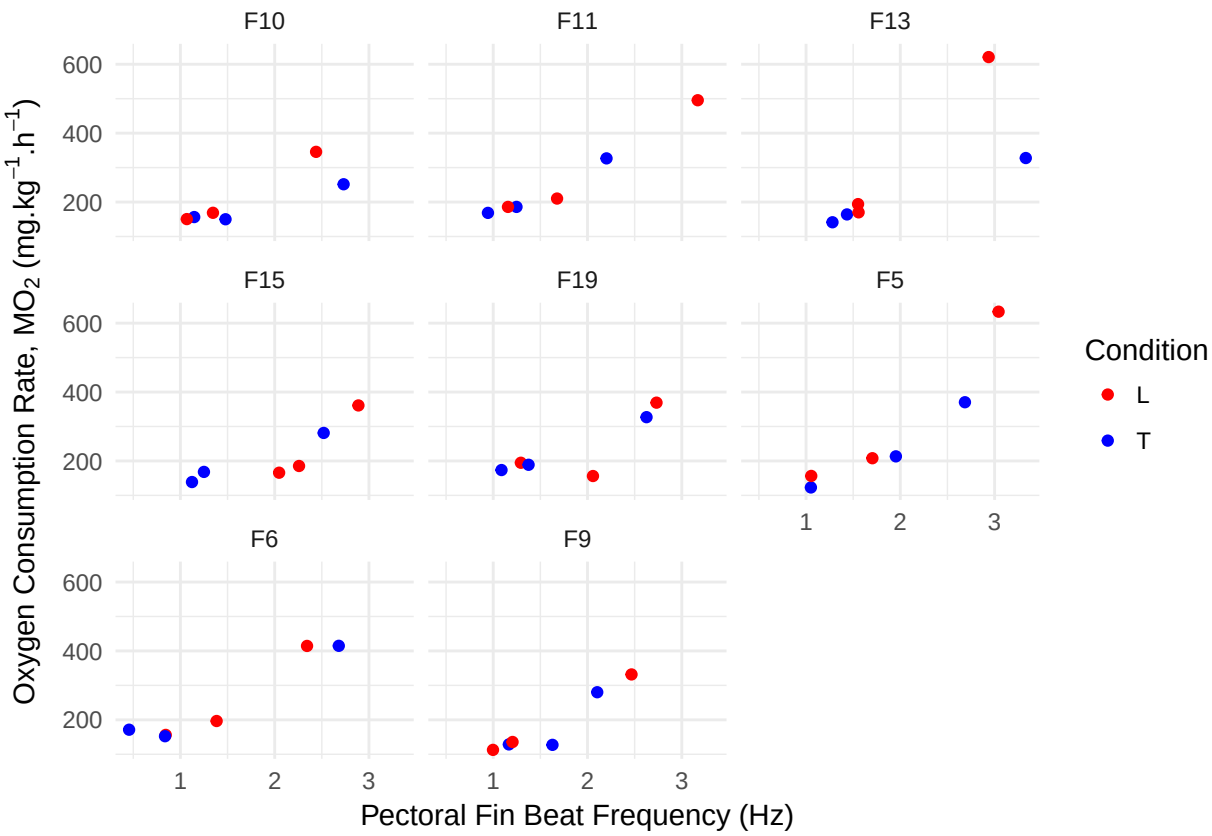


```
# Fit a GAM
library(mgcv)
```

```
## Warning: package 'mgcv' was built under R version 3.4.2
```

```
## This is mgcv 1.8-22. For overview type 'help("mgcv-package")'.
```

```
# this is fitting a model that says:
# O2 varies as a function of pectoral hz, but we should estimate a different
# curve for each condition. We also think that fish acts like a random effect
b_pec <- gam(VO2minBac~s(PecHz, cond, bs="fs") + s(Fish, bs="re"),
             data=hz, method="REML")
```

```
# check this model
gam.check(b_pec)
```

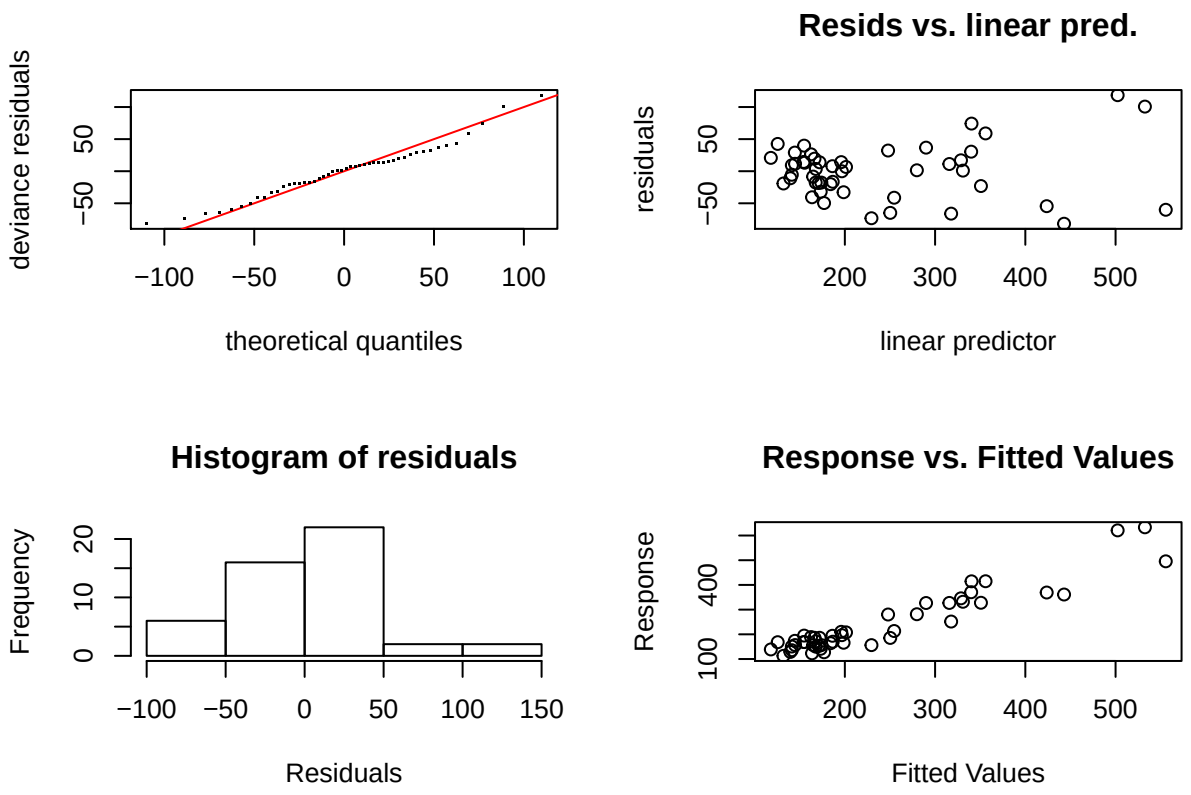


```
##
## Method: REML   Optimizer: outer newton
## full convergence after 7 iterations.
## Gradient range [-0.0001462202,0.0001143156]
## (score 264.0581 & scale 2259.291).
## Hessian positive definite, eigenvalue range [0.0001462017,24.05956].
## Model rank =  29 / 29
##
## Basis dimension (k) checking results. Low p-value (k-index<1) may
## indicate that k is too low, especially if edf is close to k'.
##
##                  k'   edf k-index p-value
## s(PecHz,cond) 20.00  6.49    0.97    0.38
## s(Fish)        8.00  4.37      NA      NA
```

```
# Little heteroskedasticity (top right). Looks like the model predicts well (bottom
# right). Residuals look normal enough (left side). Text output shows that we have
# allowed for sufficient flexibility in our model.
summary(b_pec)
```

```
##
## Family: gaussian
## Link function: identity
##
## Formula:
## VO2minBac ~ s(PecHz, cond, bs = "fs") + s(Fish, bs = "re")
```

```
##
## Parametric coefficients:
##             Estimate Std. Error t value Pr(>|t|)
## (Intercept)   222.69      63.07   3.531  0.00115 **
## ---
## Signif. codes:  0 '***' 0.001 '**' 0.01 '*' 0.05 '.' 0.1 ' ' 1
##
## Approximate significance of smooth terms:
##                 edf Ref.df      F p-value
## s(PecHz,cond) 6.489     19 15.001  <2e-16 ***
## s(Fish)       4.368      7  1.595  0.0251 *
## ---
## Signif. codes:  0 '***' 0.001 '**' 0.01 '*' 0.05 '.' 0.1 ' ' 1
##
## R-sq.(adj) =  0.852   Deviance explained = 88.6%
## -REML = 264.06  Scale est. = 2259.3    n = 48
```

```r
# v. high % deviance explained, will continue to include the fish random effect
# to explicitly include between-fish variability


# now to make predictions, make a grid of values with all the pectoral hz we need
# plus values for the condition and fish
preddat <- expand.grid(PecHz = seq(0.5, 3.5, by=0.1),
                       cond  = c("T", "L"),
                       Fish  = unique(hz$Fish))

# make predictions, also predict the standard error
pr <- predict(b_pec, preddat, type="response", se=TRUE)
preddat$VO2minBac <- pr$fit
# generate the CIs
preddat$upper <- pr$fit + 2*pr$se.fit
preddat$lower <- pr$fit - 2*pr$se.fit


# what does that look like?
p <- ggplot(hz) +
  geom_line(aes(x=PecHz, y=VO2minBac, colour=cond, group=cond), data=preddat) +
  geom_line(aes(x=PecHz, y=upper, colour=cond, group=cond), linetype=2, data=preddat) +
  geom_line(aes(x=PecHz, y=lower, colour=cond, group=cond), linetype=2, data=preddat) +
  geom_text(aes(x=PecHz, y=VO2minBac, colour=cond, label=speedcode)) +
  # scale_colour_brewer(type="qual") +
  theme_minimal() +
  scale_color_manual(values=c('blue', 'red')) +
  labs(x="Pectoral Fin Beat Frequency (Hz)", y = expression("Oxygen Consumption Rate, MO"[2]* " ("*mg.kg^{-1}*.h^{-1}*")"), colour="Condition")+
  facet_wrap(~Fish, nrow=2)

print(p)
```

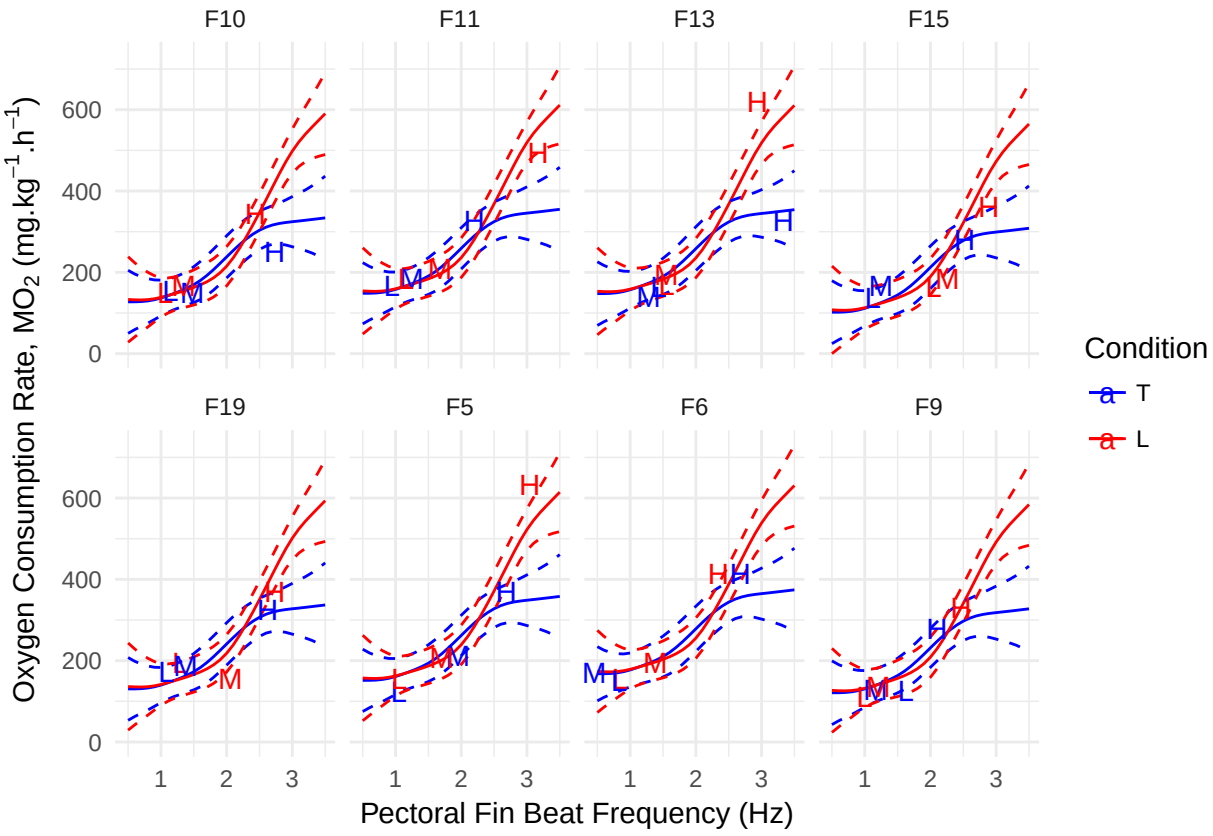


```
# ignore fish and predict integrating out the fish random effect
preddat <- expand.grid(PecHz = seq(0.5, 3.5, by=0.1),
                       cond  = c("T", "L"), Fish="F5")
pr <- predict(b_pec, preddat, type="response", se=TRUE, exclude="s(Fish)")
preddat$VO2minBac <- pr$fit
preddat$upper <- pr$fit + 2*pr$se.fit
preddat$lower <- pr$fit - 2*pr$se.fit

# what does that look like?
p <- ggplot(hz) +
  geom_line(aes(x=PecHz, y=VO2minBac, colour=cond, group=cond), data=preddat) +
  geom_line(aes(x=PecHz, y=upper, colour=cond, group=cond), linetype=2, data=preddat) +
  geom_line(aes(x=PecHz, y=lower, colour=cond, group=cond), linetype=2, data=preddat) +
  geom_text(aes(x=PecHz, y=VO2minBac, colour=cond, label=speedcode)) +
  # scale_colour_brewer(type="qual") +
  # scale_shape_manual(values=c(16, 17))+
  scale_color_manual(values=c('blue', 'red'))+
  theme_minimal() +
  labs(x="Pectoral Fin Beat Frequency (Hz)", y = expression("Oxygen Consumption Rate, MO"[2]* " ("*mg.kg^{-1}*.h^{-1}*")"), colour="Condition")

print(p)
```

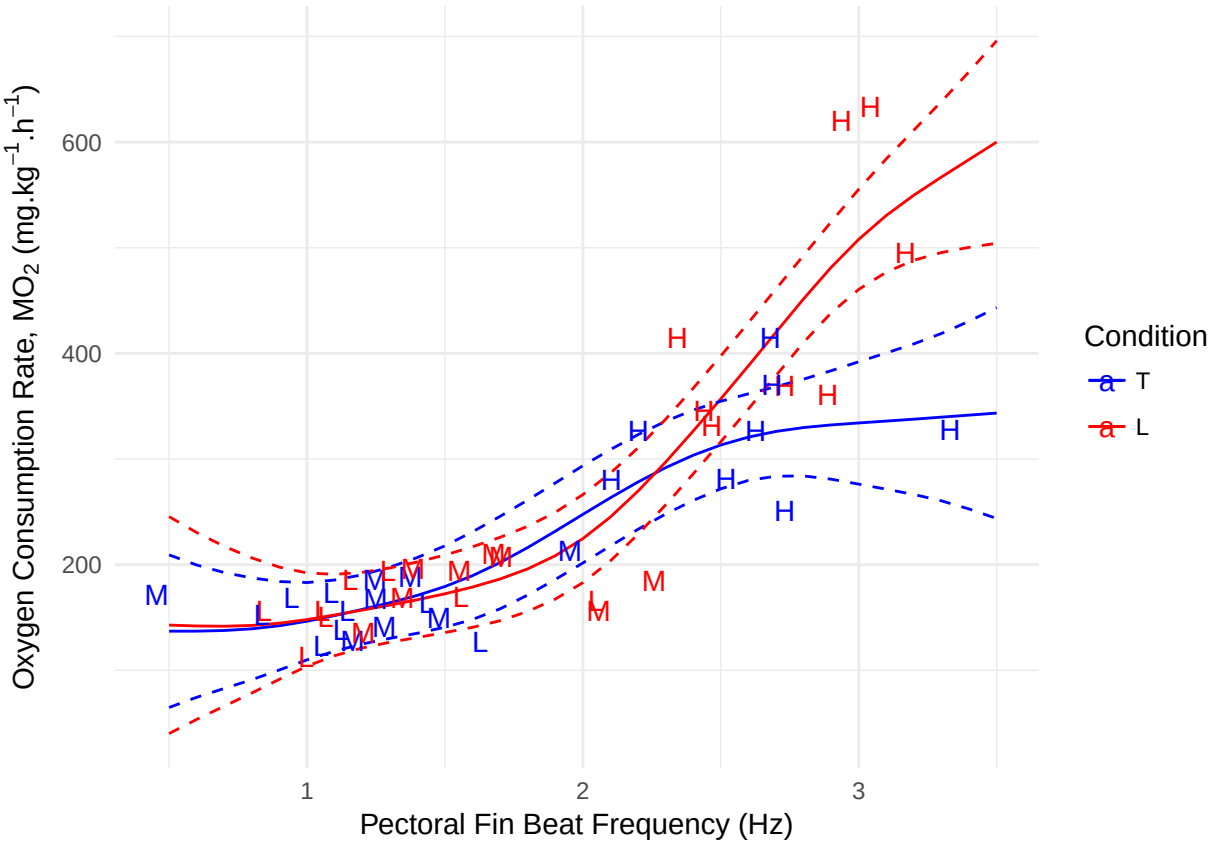

We were interested in testing the relationship between oxygen consumption and caudal fin use or frequency; however, the caudal fin was rarely used and was 0 in 65% of the experimental conditions. Model formulation and figures of the raw data are included below to illustrate the limitations of the data and the observed caudal fin use patterns.

```
# quick visualisation
p <- ggplot(hz) +
  geom_point(aes(x=CaudHz, y=VO2minBac, colour=cond)) +
  theme_minimal() +
  scale_shape_manual(values=c(16, 17)) +
  scale_color_manual(values=c('red', 'blue')) +
  labs(x="Caudal Fin Beat Frequency (Hz)", y = expression("Oxygen Consumption Rate, MO"[2]* " ("*mg.kg^{-1}*.h^{-1}*")"), colour="Condition") +
  facet_wrap(~Fish)

print(p)
```

```
## Warning: Removed 1 rows containing missing values (geom_point).
```

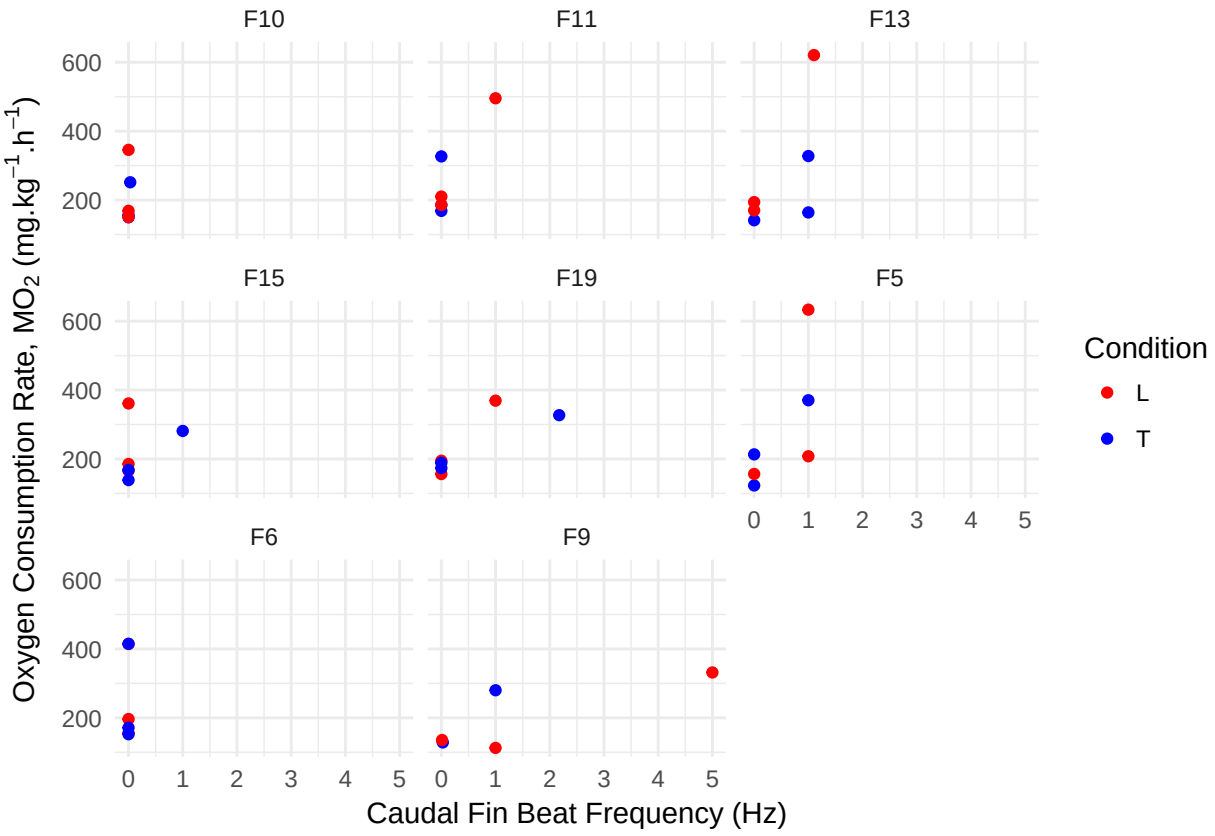


```
# try the same kind of model as above for the caudal fin frequency
# need to reduce k (smooth complexity) as we don't have many unique values
b_caud <- gam(VO2minBac~s(CaudHz, cond, bs="fs", k=5) + s(Fish, bs="re"),
              data=hz, method="REML")

# model check
summary(b_caud)
```

```
##
## Family: gaussian
## Link function: identity
##
## Formula:
## VO2minBac ~ s(CaudHz, cond, bs = "fs", k = 5) + s(Fish, bs = "re")
##
## Parametric coefficients:
##             Estimate Std. Error t value Pr(>|t|)
## (Intercept)    458.9      105.8   4.338  8.7e-05 ***
## ---
## Signif. codes:  0 '***' 0.001 '**' 0.01 '*' 0.05 '.' 0.1 ' ' 1
##
## Approximate significance of smooth terms:
##                       edf Ref.df     F p-value
## s(CaudHz,cond) 3.555e+00      8 2.311 0.00123 **
## s(Fish)        7.269e-05      7 0.000 0.66065
## ---
## Signif. codes:  0 '***' 0.001 '**' 0.01 '*' 0.05 '.' 0.1 ' ' 1
##
```

```
## R-sq.(adj) =  0.287   Deviance explained = 34.2%
## -REML = 285.97  Scale est. = 10942     n = 47
```

```
# less deviance explained than before
plot(b_caud)
```

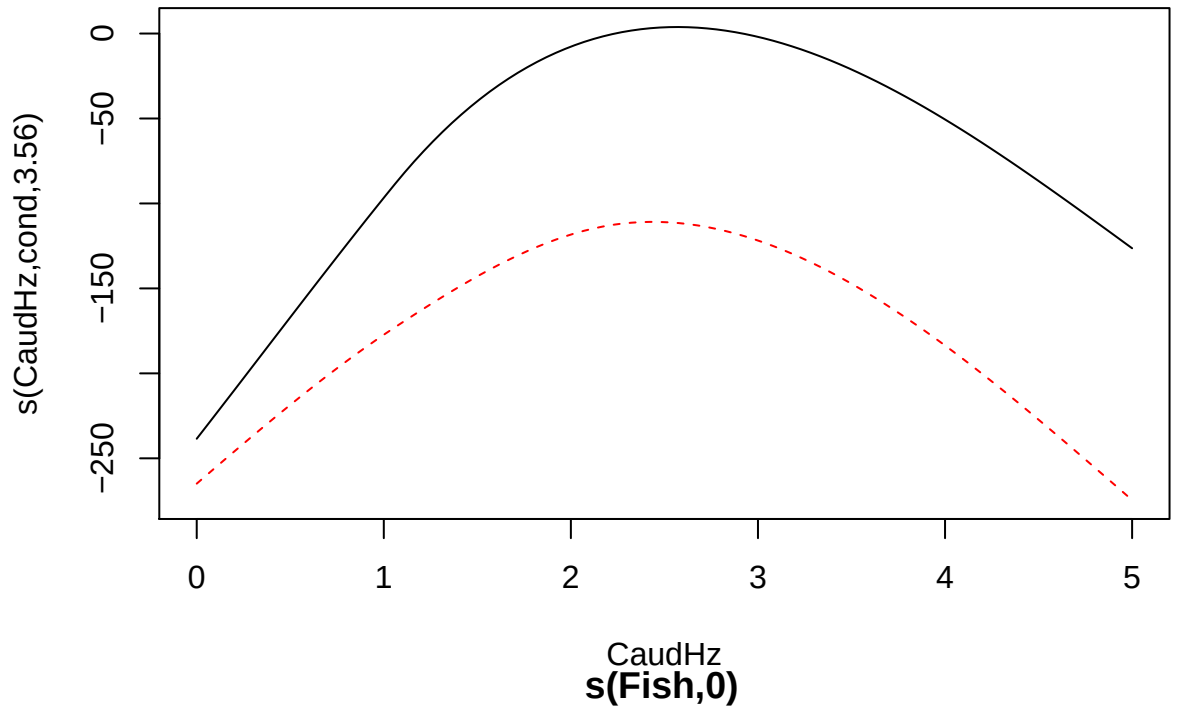

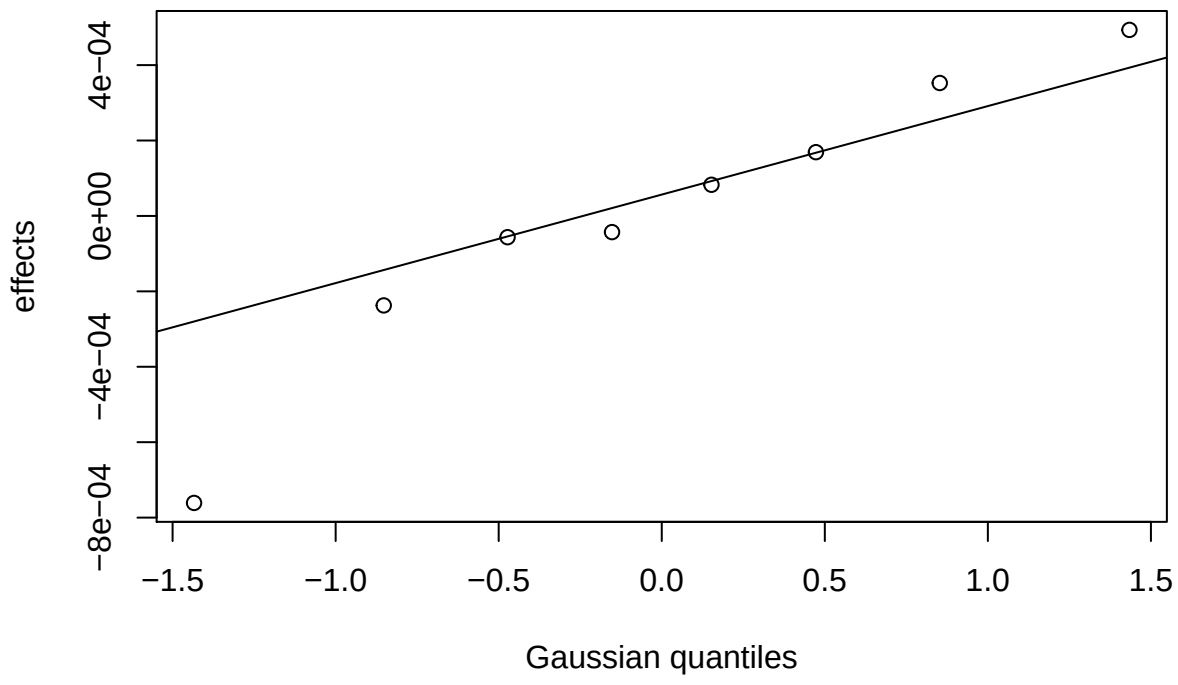


```
# do we believe that O2 is n-shaped in caudal hz? Unlikely
```

```
preddat <- expand.grid(CaudHz = seq(0, 5, by=0.1),
                       cond  = c("T", "L"),
                       Fish  = unique(hz$Fish))

preddat$VO2minBac <- predict(b_caud, preddat, type="response")


p <- ggplot(hz) +
  geom_line(aes(x=CaudHz, y=VO2minBac, colour=cond, group=cond), data=preddat) +
  geom_text(aes(x=CaudHz, y=VO2minBac, colour=cond, label=speedcode)) +
  # scale_colour_brewer(type="qual") +
  theme_minimal() +
  labs(x="Caudal Hz", colour="Condition") +
  scale_shape_manual(values=c(16, 17)) +
  scale_color_manual(values=c('red', 'blue')) +
  labs(x="Caudal Fin Beat Frequency (Hz)", y = expression("Oxygen Consumption Rate, MO"[2]* " ("*mg.kg^{-1}*.h^{-1}*")"), colour="Condition") +
  facet_wrap(~Fish, nrow=2)

print(p)
```

```
## Warning: Removed 1 rows containing missing values (geom_text).
```

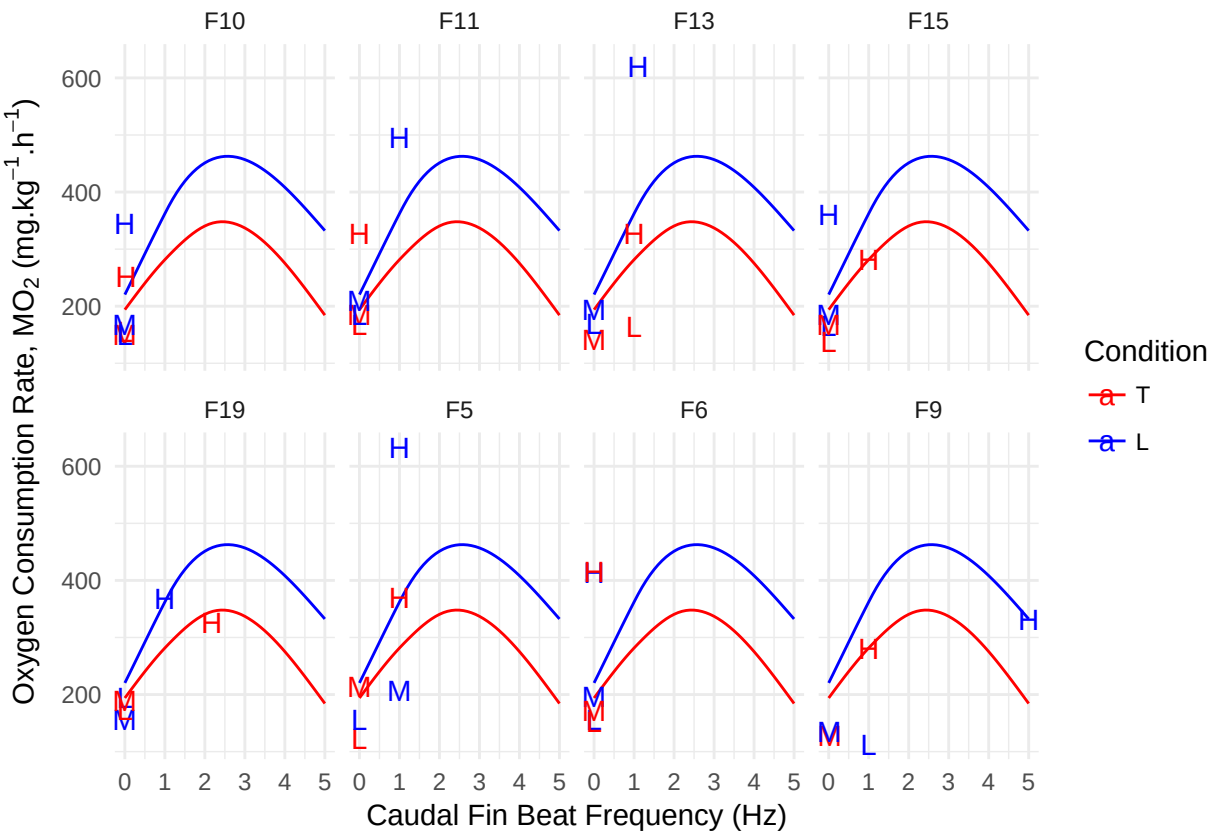


```
## what about caudal use? Will have the same data limitation (when Hz = 0, use = 0)

# quick visualisation
p <- ggplot(hz) +
  geom_point(aes(x=Cauduse, y=VO2minBac, colour=cond)) +
```

```
  theme_minimal() +
  scale_shape_manual(values=c(16, 17)) +
  scale_color_manual(values=c('red', 'blue')) +
  labs(x="Caudal Fin Use (%)", y = expression("Oxygen Consumption Rate, MO"[2]* " ("*mg.kg^{-1}*.h^{-1}*")"), colour="Condition") +
  facet_wrap(~Fish)

print(p)
```

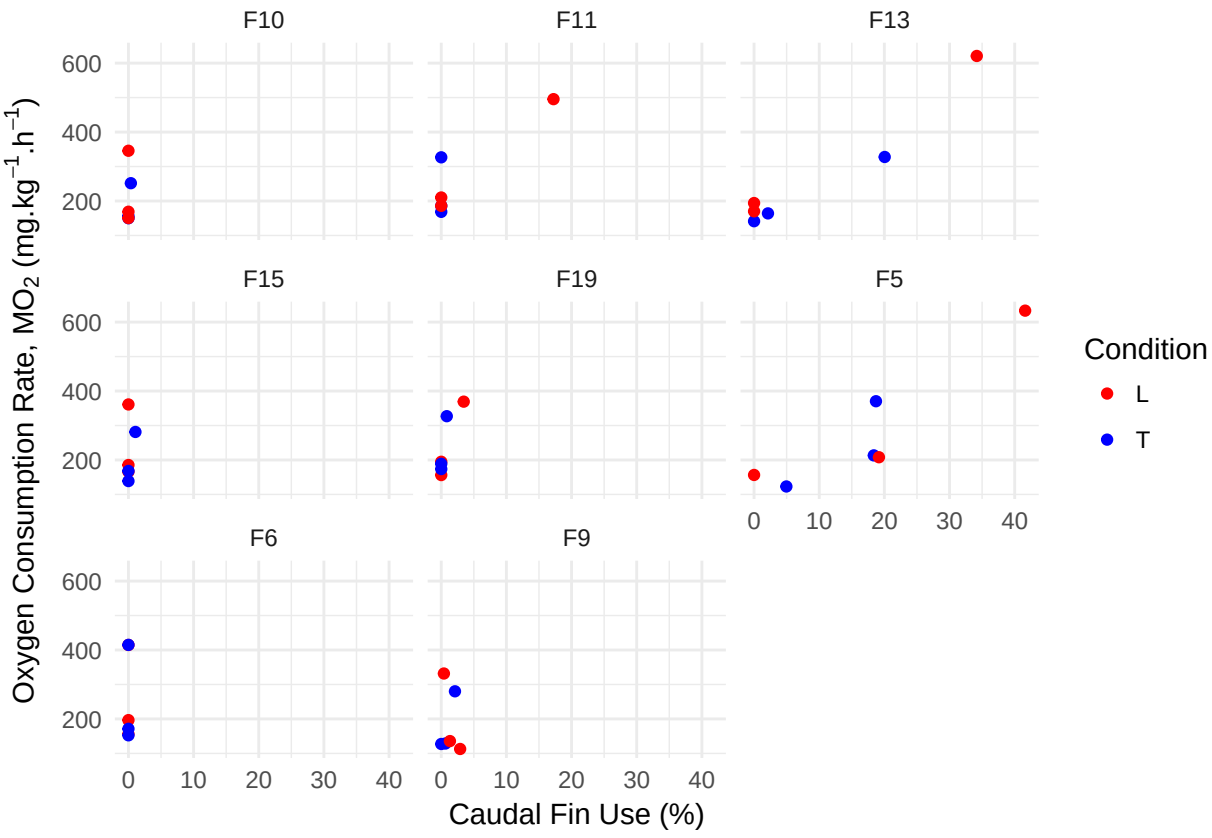


```
# try the same kind of model as above for the caudal fin use
# need to reduce k (smooth complexity) as we don't have many unique values
b_caud <- gam(VO2minBac~s(Cauduse, cond, bs="fs", k=5) + s(Fish, bs="re"),
              data=hz, method="REML")

# model check
summary(b_caud)
```

```
##
## Family: gaussian
## Link function: identity
##
## Formula:
## VO2minBac ~ s(Cauduse, cond, bs = "fs", k = 5) + s(Fish, bs = "re")
##
## Parametric coefficients:
##             Estimate Std. Error t value Pr(>|t|)
## (Intercept)   235.85      17.24   13.68   <2e-16 ***
## ---
```

```
## Signif. codes:  0 '***' 0.001 '**' 0.01 '*' 0.05 '.' 0.1 ' ' 1
##
## Approximate significance of smooth terms:
##                       edf Ref.df    F  p-value
## s(Cauduse,cond) 2.288983      9 4.73 5.49e-08 ***
## s(Fish)         0.001065      7 0.00    0.532
## ---
## Signif. codes:  0 '***' 0.001 '**' 0.01 '*' 0.05 '.' 0.1 ' ' 1
##
## R-sq.(adj) =  0.475   Deviance explained = 50.1%
## -REML = 282.88  Scale est. = 8019.5    n = 48
```

```
# less deviance explained than before
plot(b_caud)
```

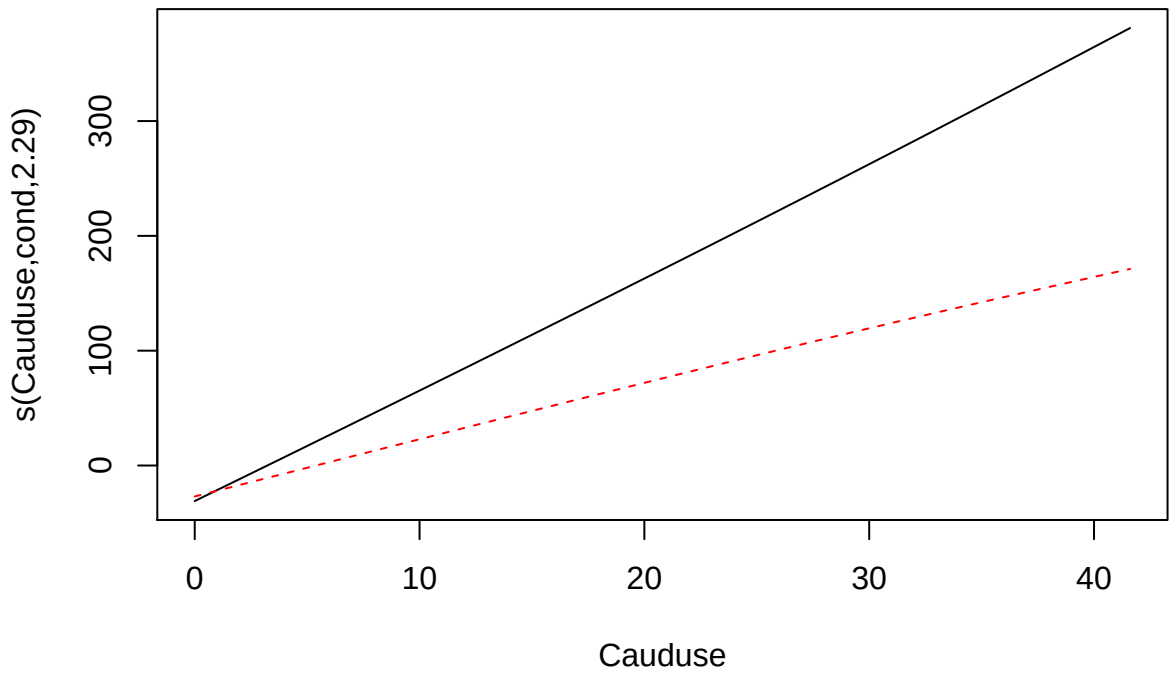

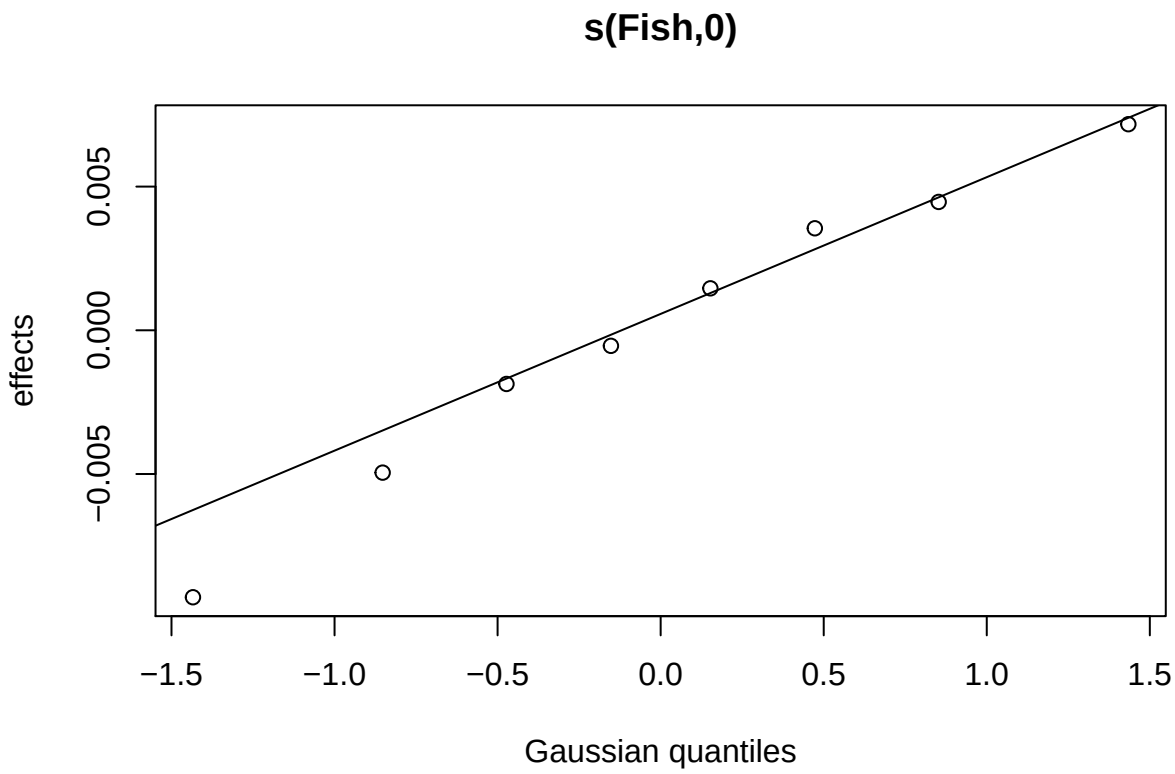


```
# do we believe that O2 is n-shaped in caudal hz? Unlikely


preddat <- expand.grid(Cauduse = seq(0, 45, by=1),
                       cond  = c("T", "L"),
                       Fish  = unique(hz$Fish))

preddat$VO2minBac <- predict(b_caud, preddat, type="response")


p <- ggplot(hz) +
  geom_line(aes(x=Cauduse, y=VO2minBac, colour=cond, group=cond), data=preddat) +
  geom_text(aes(x=Cauduse, y=VO2minBac, colour=cond, label=speedcode)) +
  # scale_colour_brewer(type="qual") +
  theme_minimal() +
  labs(x="Caudal Hz", colour="Condition") +
  scale_shape_manual(values=c(16, 17)) +
  scale_color_manual(values=c('red', 'blue')) +
  labs(x="Caudal Fin Use (%)", y = expression("Oxygen Consumption Rate, MO"[2]* " ("*mg.kg^{-1}*.h^{-1}*")"), colour="Condition") +
  facet_wrap(~Fish, nrow=2)

print(p)
```

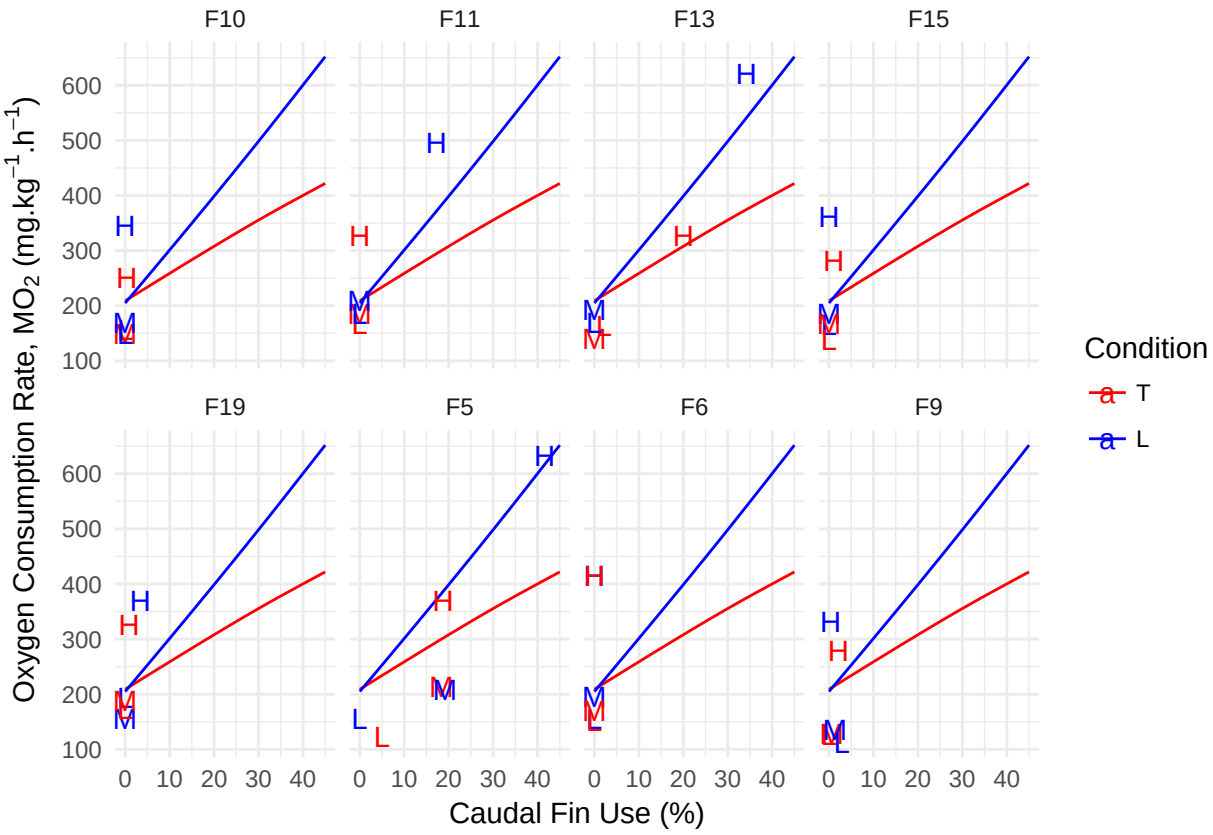


```
## and CV of pectoral fin beat frequency (following Roche et al. 2014)
# quick visualisation
p <- ggplot(hz) +
  geom_point(aes(x=CV.Pec, y=VO2minBac, colour=cond)) +
  theme_minimal() +
  scale_shape_manual(values=c(16, 17)) +
  scale_color_manual(values=c('red', 'blue')) +
  labs(x="CV of Pectoral Fin Beat Frequency", y = expression("Oxygen Consumption Rate, MO"[2]* " ("*mg.kg^{-1}*.h^{-1}*")"), colour="Condition") +
  facet_wrap(~Fish)

print(p)
```

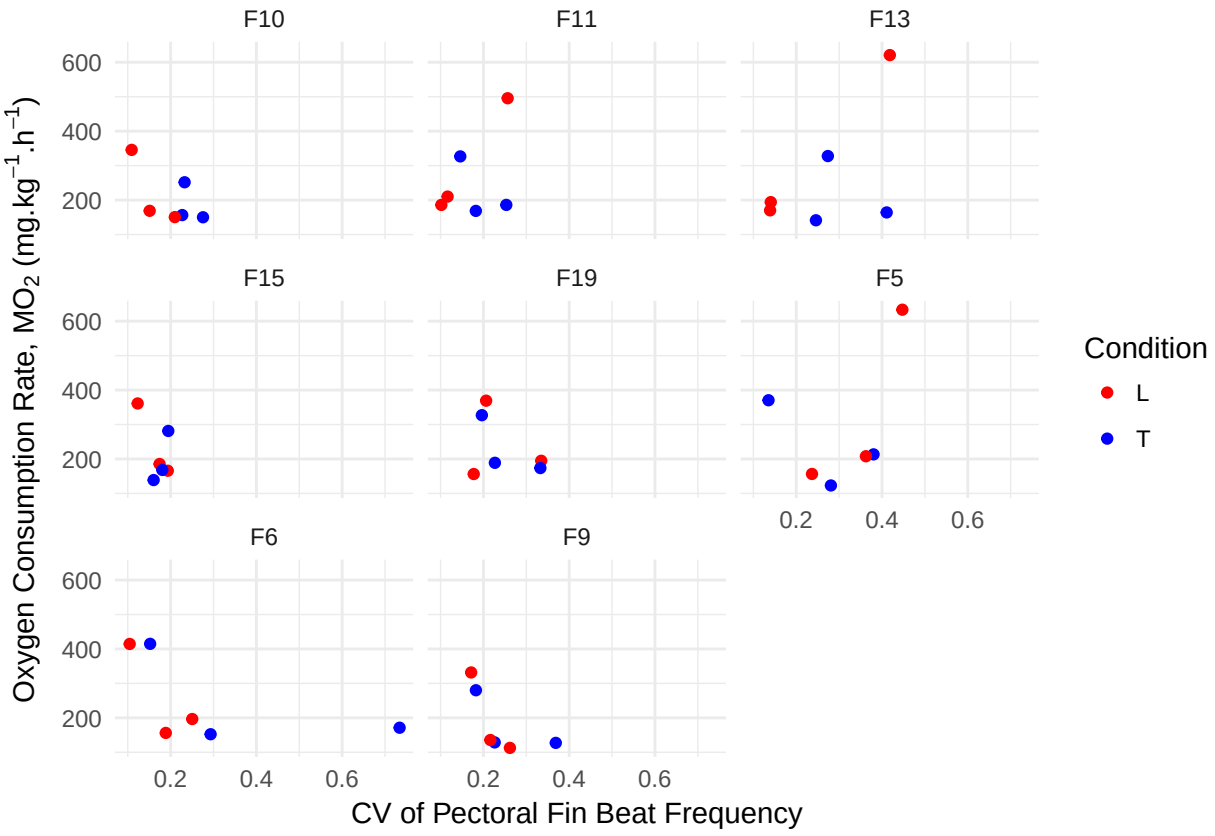


```
# try the same kind of model as above for the caudal fin use
# need to reduce k (smooth complexity) as we don't have many unique values
b_cvpec <- gam(VO2minBac~s(CV.Pec, cond, bs="fs", k=5) + s(Fish, bs="re"),
               data=hz, method="REML")

# model check
summary(b_cvpec)
```

```
##
## Family: gaussian
## Link function: identity
##
## Formula:
## VO2minBac ~ s(CV.Pec, cond, bs = "fs", k = 5) + s(Fish, bs = "re")
##
## Parametric coefficients:
##             Estimate Std. Error t value Pr(>|t|)
## (Intercept)   180.79      95.78   1.888    0.066 .
## ---
## Signif. codes:  0 '***' 0.001 '**' 0.01 '*' 0.05 '.' 0.1 ' ' 1
##
## Approximate significance of smooth terms:
##                       edf Ref.df    F  p-value
## s(CV.Pec,cond) 4.8544608      9 3.29 0.000121 ***
## s(Fish)        0.0004511      7 0.00 0.947203
## ---
## Signif. codes:  0 '***' 0.001 '**' 0.01 '*' 0.05 '.' 0.1 ' ' 1
##
```

```
## R-sq.(adj) =  0.387   Deviance explained =   45%
## -REML = 290.95  Scale est. = 9375.6    n = 48
```

```
# less deviance explained than before
plot(b_cvpec)
```

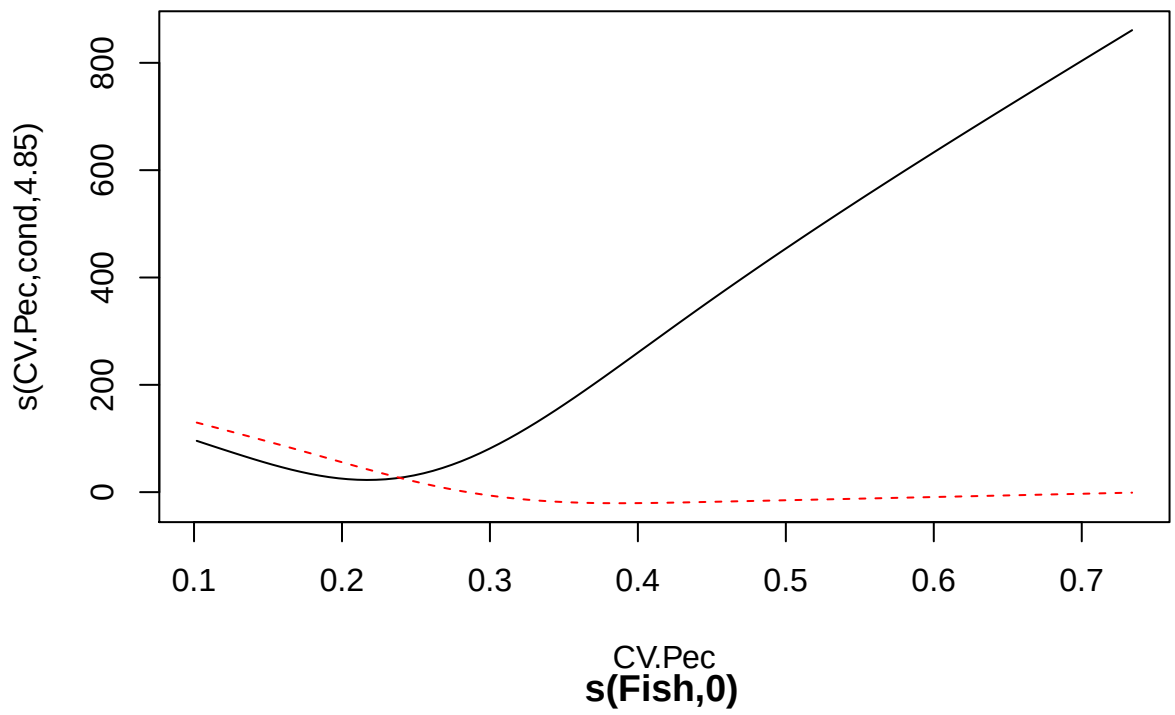


```
# do we believe that O2 is n-shaped in caudal hz? Unlikely
```

```
preddat <- expand.grid(CV.Pec = seq(0, 0.75, by=0.1),
                       cond  = c("T", "L"),
                       Fish  = unique(hz$Fish))

preddat$VO2minBac <- predict(b_cvpec, preddat, type="response")


p <- ggplot(hz) +
  geom_line(aes(x=CV.Pec, y=VO2minBac, colour=cond, group=cond), data=preddat) +
  geom_text(aes(x=CV.Pec, y=VO2minBac, colour=cond, label=speedcode)) +
  # scale_colour_brewer(type="qual") +
  theme_minimal() +
  # scale_shape_manual(values=c(16, 17)) +
  scale_color_manual(values=c('blue', 'red')) +
  labs(x="CV of Pectoral Fin Beat Frequency", y = expression("Oxygen Consumption Rate, MO"[2]* " ("*mg.kg^{-1}*.h^{-1}*")"), colour="Condition") +
  facet_wrap(~Fish, nrow=2)

print(p)
```

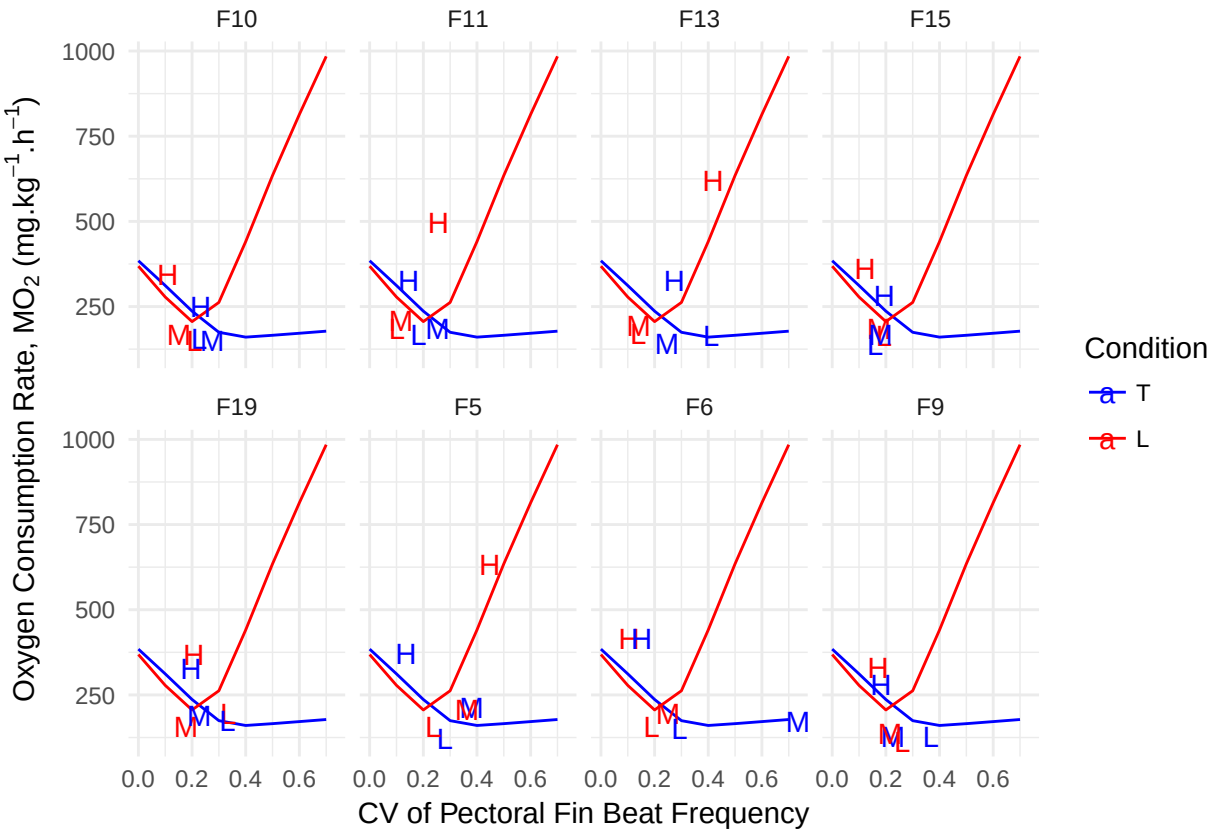


```
# plot all together by integrating out fish random effect
preddat <- expand.grid(CV.Pec = seq(0, 0.75, by=0.1),
                       cond  = c("T", "L"), Fish="F5")
pr <- predict(b_cvpec, preddat, type="response", se=TRUE, exclude="s(Fish)")
preddat$VO2minBac <- pr$fit
preddat$upper <- pr$fit + 2*pr$se.fit
preddat$lower <- pr$fit - 2*pr$se.fit
```

```
# what does that look like?
p <- ggplot(hz) +
  geom_line(aes(x=CV.Pec, y=VO2minBac, colour=cond, group=cond), data=preddat) +
  geom_line(aes(x=CV.Pec, y=upper, colour=cond, group=cond), linetype=2, data=preddat) +
  geom_line(aes(x=CV.Pec, y=lower, colour=cond, group=cond), linetype=2, data=preddat) +
  geom_text(aes(x=CV.Pec, y=VO2minBac, colour=cond, label=speedcode)) +
  # scale_colour_brewer(type="qual") +
  # scale_shape_manual(values=c(16, 17))+
  scale_color_manual(values=c('blue', 'red'))+
  theme_minimal() +
  labs(x="CV of Pectoral Fin Beat Frequency", y = expression("Oxygen Consumption Rate, MO"[2]* " ("*mg.kg^{-1}*.h^{-1}*")"), colour="Condition")

print(p)
```

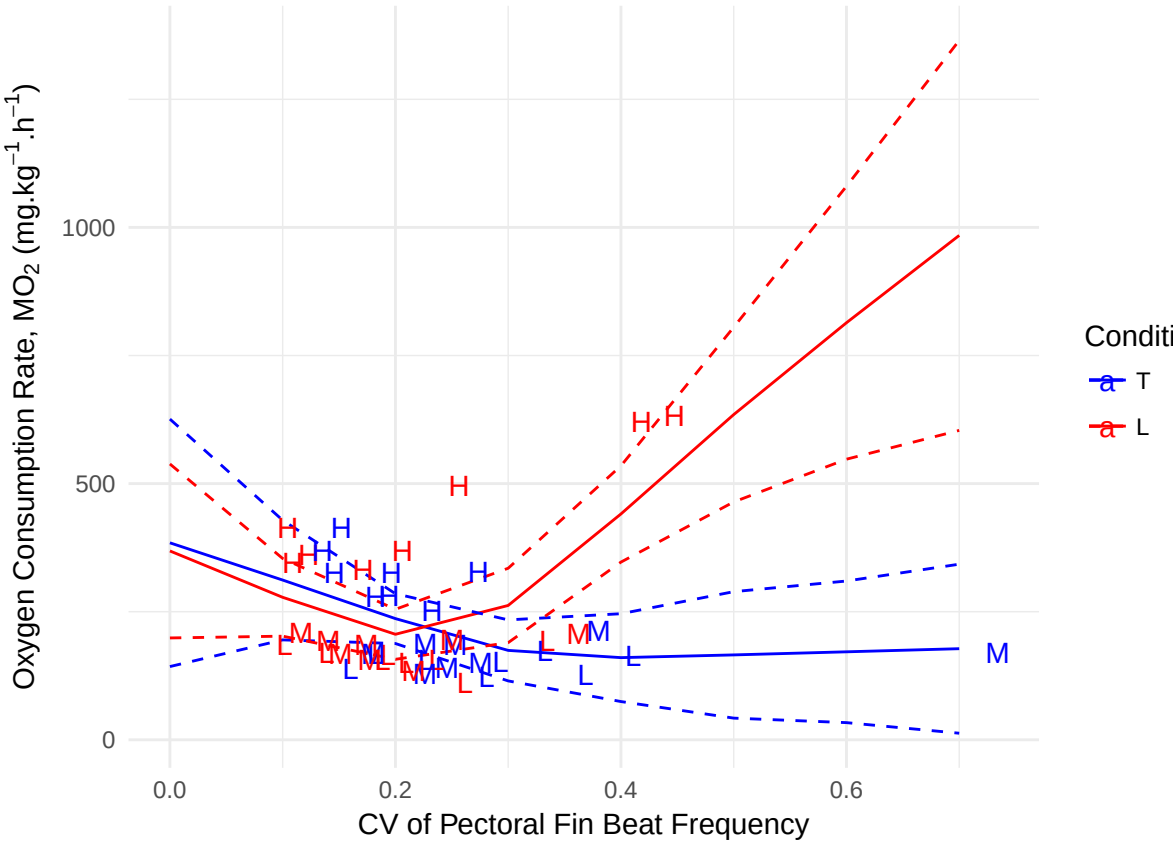

To investigate the position of fish in the tank, we compared the centroid locations of the snout of each fish through the 180s sample period, and standard deviation from that centroid position, in different speed*flow combinations. This investigation along with the heatmaps (Figure 5) illustrate the overall positioning of individuals within the tank; however our interpretation is limited due to the number of response parameters compared to the number of animals tested and the factors to be considered.